Relationship of Mechanical Deformations and Electrochemical Properties of Lithium Ion Batteries-An Experimental Study

by

Christopher M.A. Reynolds

B.S., Mechanical Engineering, United States Naval Academy, 2014

Submitted to the Department of Mechanical Engineering
in Partial Fulfillment of the Requirements for the Degrees of

Naval Engineer

and

Master of Science in Mechanical Engineering

at the

Massachusetts Institute of Technology
May 2022

Signature of the Author……
Department of Mechanical Engineering
May 2022

Certified by……
Tomasz Wierzbicki
Professor of Applied Mechanics, Department of Mechanical Engineering
Thesis Supervisor

Accepted by……...
Nicolas Hadjiconstantinou
Chairman, Department Committee on Graduate Students
Department of Mechanical Engineering

Relationship of Mechanical Deformations and Electrochemical Properties of Lithium Ion Batteries-An Experimental Study

by

Christopher M.A. Reynolds

Submitted to the Department of Mechanical Engineering
on May 6th, 2021, for partial fulfillment of the
requirements for the degrees of
Naval Engineer
and
Master of Science in Mechanical Engineering

Abstract

MIT's Impact & Crashworthiness Lab (ICL) has been conducting research into lithium-ion batteries in an effort to produce a computation model that can predict the impact of mechanical deformations on electrochemical properties of lithium-ion batteries. Experiments were conducted on two different types of lithium-ion battery cells in order to continue gathering data to refine and validate the ICL model. First, prismatic cells were cycled through a various number of charges and discharges, with one prismatic cell placed under a compressive load to measure how much force it would exert on its carriage throughout its cycling. Upon completion of the cycling, the prismatic cells were subjected to indentation to the point of mechanical failure. Second, pouch cells were subjected to three different four-point bending conditions, and cycled through 10 charges and discharges. Upon completion of the cycling, the pouch cells were removed from the four-point bending system to measure the deflection of the changed shape. Various voltage, current, and force measurements were taken throughout the experiments to help refine the ICL computational model, as well as allowing for additional observations to be made regarding the relationship between mechanical deformations and electrochemical properties.

Thesis Supervisor: Tomasz Wierzbicki
Title: Professor of Applied Mechanics, Department of Mechanical Engineering

Contents

List of Figures

List of Tables

Chapter 1: Introduction

1.1: Brief Overview of Lithium-Ion Batteries

Lithium-ion batteries are widely used in portable electronics, power tools, and electric vehicles, due to their advantages over other types of batteries. These advantages include recharge-ability, high energy densities, and minimal to no memory effects. While research into lithium-ion batteries first began in the 1960s by a multitude of interested parties, it wasn't until 1991 that Sony introduced the first commercially available lithium-ion battery. [1] Most lithium-ion batteries in use today have a positive electrode made of a lithium-metal oxide, a negative electrode made of a carbon material, and an electrolyte that is dependent on the ultimate use of the battery. Choices for the electrolyte include organic solvents, polymers, ionic liquids, and inorganic solids. [1] However, despite their use for the past 60 years, the technology is far from perfect. The liquid electrolytes present considerable safety risks due to their flammability and the potential to leak out of the battery. [2] Additionally, the use of organic solvents (the most common solvent used) with a lithium metal anode can promote the growth of dendrites within the battery, eventually leading to internal shorts that increase the chance of thermal runaway (a condition where the battery enters a self-heating, uncontrollable state) occurring. [3] Despite these risks, global interest in lithium-ion batteries remains at a high level for various reasons.

1.2: Global Interests in Lithium-Ion Batteries

Global interests in advancing lithium-ion battery technology are driven primarily through environmental and energy concerns, such as climate change, battery recycling, and electrification of fossil fuel driven vehicles. Climate change is primarily driven by greenhouse gases, which will continue to rise as the world continues to develop and thus consume more energy. While renewable energy is on the rise, one problem associated with it is that peak energy supply (for example, daytime for solar panels) may not necessarily correspond with peak energy demand. Lithium-ion batteries offer a solution of storing the extra energy in order to provide it at a later point, but are currently very expensive for such large scales. One possible method to reduce this cost is the use of recycled batteries, which is its own large area of research. As the demand for lithium-ion batteries increase, there are concerns about the environmental impact of mining the required materials and discarding of used batteries. Finding ways to recycle these lithium-ion batteries could reduce these impacts while satisfying the increased demand. Part of the increased demand

can be traced to the continued success of hybrid cars and rise of Tesla, which has proven the feasibility of electric cars. This has prompted other automotive manufactures to develop their own electric cars, as well as prompting other companies and entities into trying to electrify other vehicles such as airplanes and ships.

1.1: US Navy Interest in Lithium-Ion Batteries

The US Navy has a vested interest in utilizing lithium-ion batteries due to the inherent advantages previously described. However, due to the potential for ruptures and explosions, the US Navy classifies all lithium batteries as hazardous at all times. [4] Additionally, the Lithium Battery Safety Program was established to provide safety guidelines for all phases of lithium-ion battery use, set conditions for minimizing risks from the use of lithium-ion batteries, and provide a certification process for to ensure these guidelines are followed and conditions are met. [4] Despite these steps, the US Navy has still had problems with lithium-ion batteries, such as the failed Advanced Seal Delivery System (ASDS). The ASDS was a lithium-ion battery powered mini-submersible meant to deploy special forces to conduct clandestine missions. While the mini-sub was plagued by many problems during the course of its design and construction, the program was ultimately cancelled after the initial prototype caught on fire (which lasted for six hours) while charging. [5] [6] However, there are examples of successful use of lithium-ion batteries, such as Japan recently commissioning two different lithium-ion powered submarines, the Ouryu and the Taigei. [7] [8]

1.2: Previous 2N Work in the Impact & Crashworthiness Laboratory

Due to interest of the US Navy in lithium-ion batteries, previous 2N Naval Construction & Engineering students have conducted research with the Impact & Crashworthiness Laboratory (ICL). In 2017, LT Amber Mason conducted testing to refine and validate ICL's computational model for predicting the impact of mechanical deformation on the electrochemical properties of lithium-ion batteries. This testing consisted of hemispherical punch testing, internal short circuiting, material characterization, and buckling responses. [5] LT Nathaniel Byrd continued this validation in 2018 by conducting testing to determine the failure mechanism of internal battery components when subjected to out-of-plane compression and in-plane tension. [6] To continue this work, testing was performed on prismatic and pouch cells to continue refining and validating the ICL computational model.

Chapter 2: Prismatic Cell Indentation

2.1: Prismatic Cell & Experimental Description

Four prismatic type lithium ion cells, pictured in Figure 2-1, were used for this study. Table 2.1 list the relevant dimensions and properties of the cells. These prismatic cells were brand new and had been sent to the ICL by one of its corporate sponsors.

Figure 2-1: Lithium-Ion Prismatic Cell

Property	Value
Nominal Capacity	40Ah
Nominal Voltage	3.5V
Height	9.2 cm
Length	15 cm
Thickness	3 cm

Table 2.1: Lithium-Ion Prismatic Cell Properties

An MTI 4-Channel Battery Analyzer, shown in Figure 2-2, was used to charge and discharge the prismatic cells throughout the testing. One of the batteries was subjected to a compression load throughout its cycling using an Instron 5944 loading frame, shown in Figure 2-3.

Figure 2-2: MTI Corporation 4-Channel Battery Analyzer with Control Laptop [1]

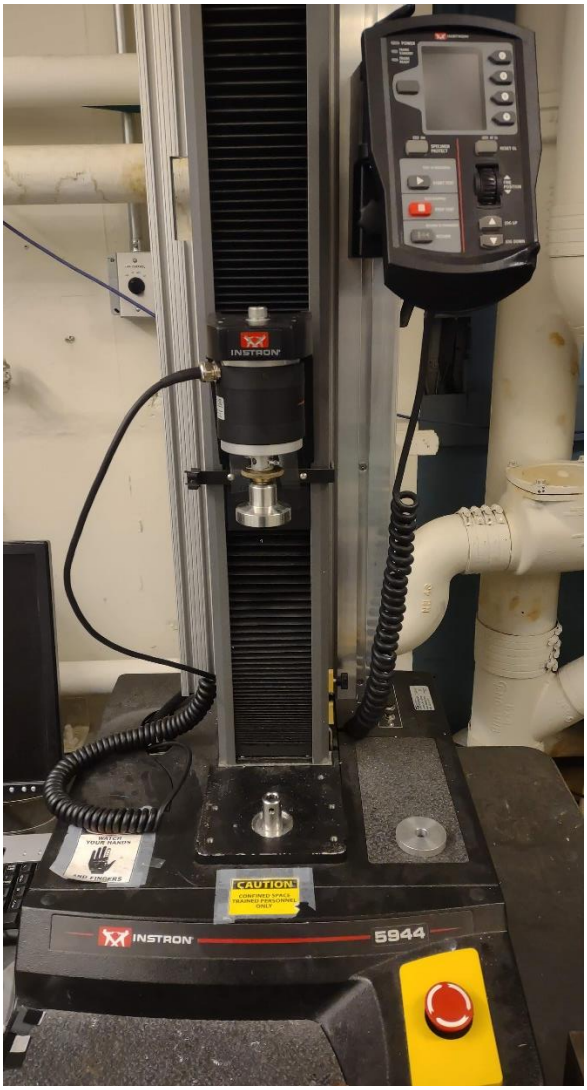

Figure 2-3: Instron 5944 Loading Frame

Upon completion of the cycling, the batteries were indented using a 200 kN load cell on an MTS loading frame, shown in Figure 2-4. The indentation stopped once the batteries were thoroughly damaged and short circuited. The damage was indicated visual inspection and a sharp drop in the force applied by the MTS loading frame, while the short circuit was indicated by a sudden voltage drop to zero.

Figure 2-4: MTS Loading Frame [2]

2.2: Experiment Setup & Method

2.2.1: Testing Rig Development

In preparation for the experiments, three testing rigs were designed and manufactured as the terminals on the prismatic cells were not compatible with the cables from the battery analyzer. One testing rig, shown in Figure 2-5, consisted of a battery cradle and two electrical connectors. The schematics for the battery cradle and electrical connectors are shown in Figure 2-6 and Figure 2-7, respectively.

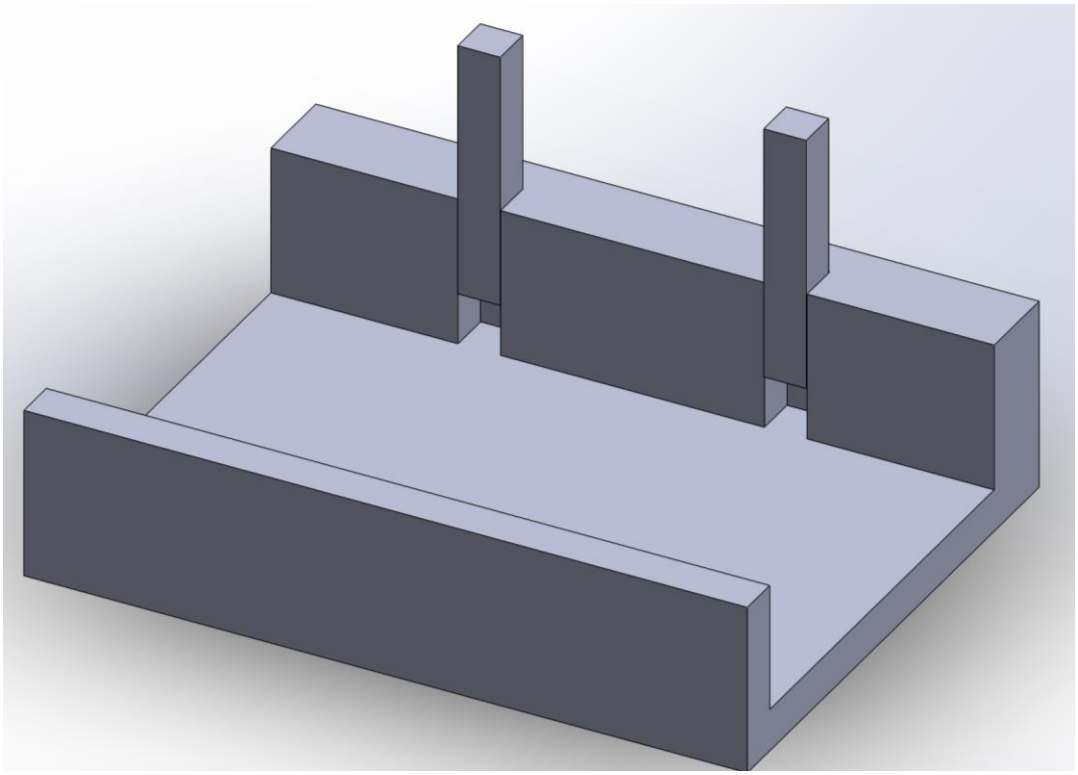

Figure 2-5: Testing Rig

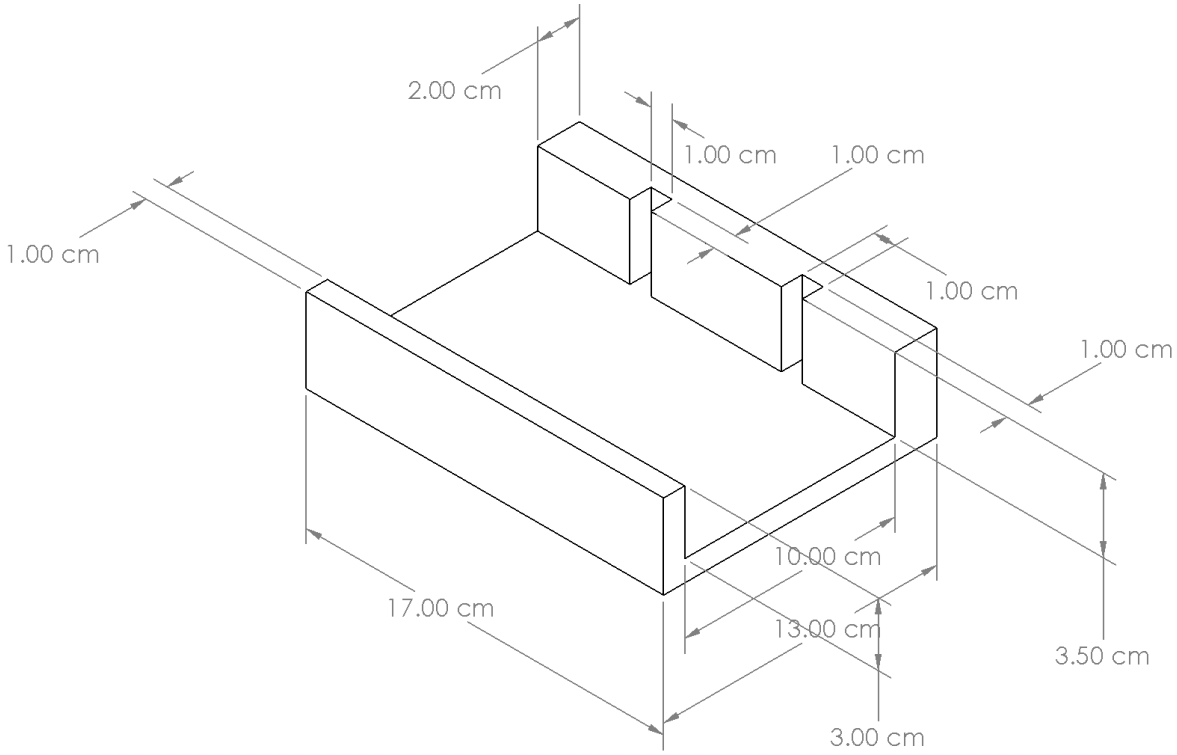

Figure 2-6: Battery Cradle Schematic

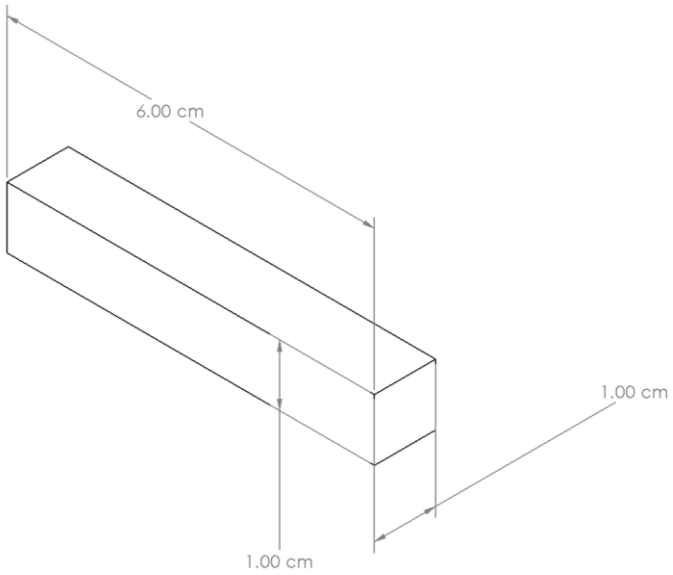

Figure 2-7: Electrical Connector Schematic

Additionally, one of the testing rigs had a flat plate that was placed on top of the battery that was subjected to compression loading while cycling. Figure 2-8 shows the schematic for the flat plate, while Figure 2-9 shows how it fit into the testing rig.

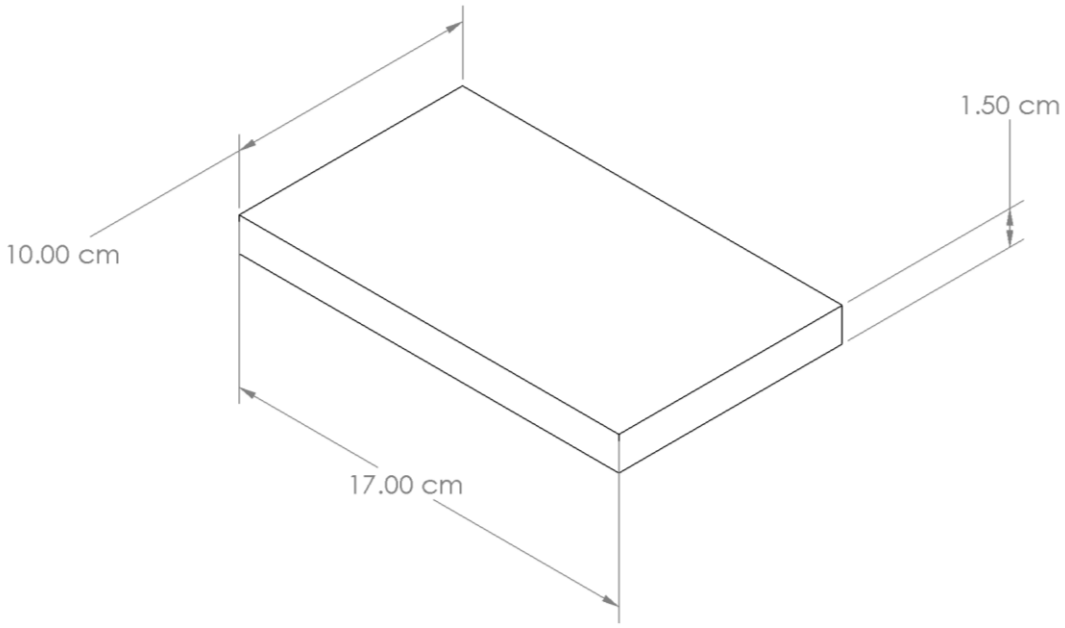

Figure 2-8: Flat Plate Schematic

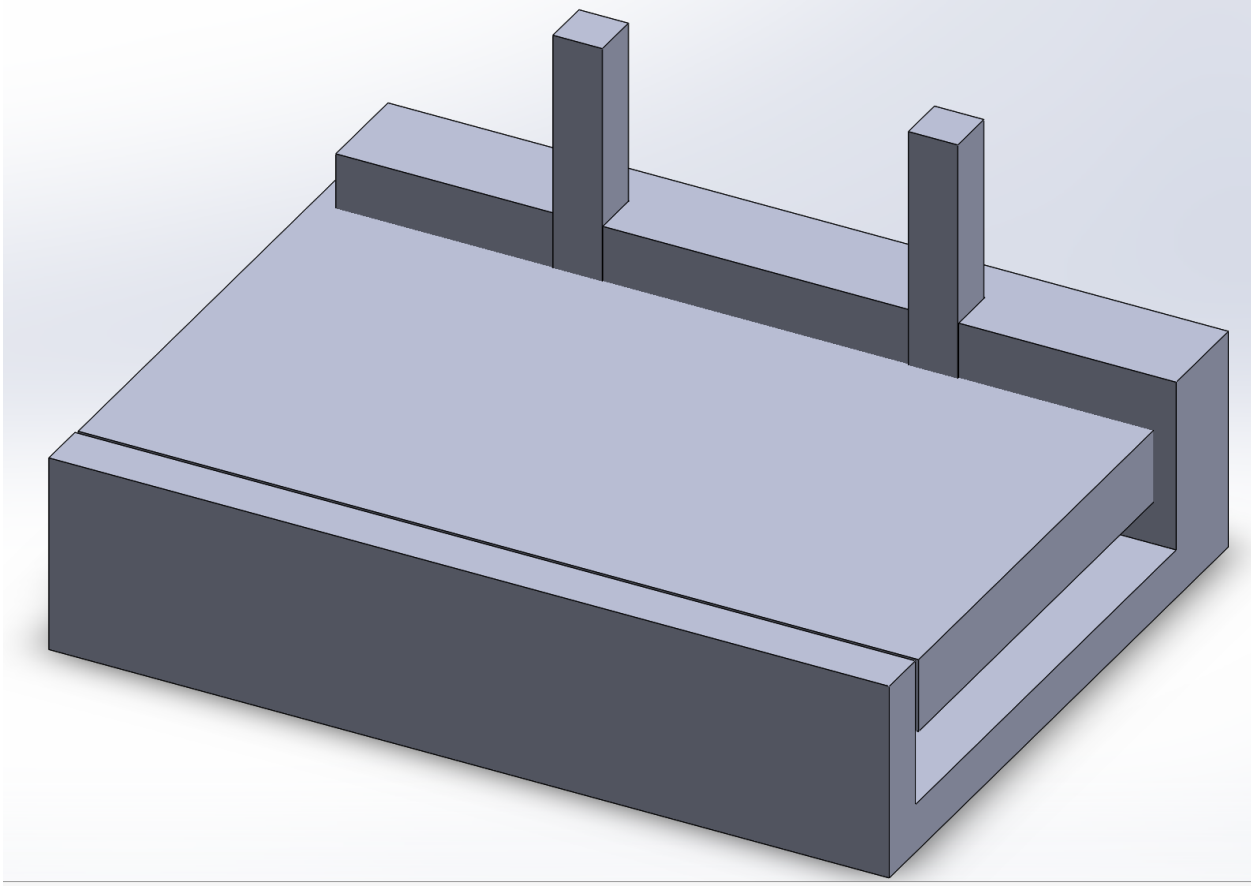

Figure 2-9: Testing Rig with Flat Plate

2.2.2: Experiment Procedure

Upon completing of the testing rigs, three batteries (Batteries 1, 2, and 3) were cycled various amounts, while a fourth battery was not cycled at all in order to act as a control for the other batteries. A single cycle is defined in Table 2.2, and associated voltage and current are plotted in Figure 2-10:

Cycle Step #	Cycle Step
1	Constant Current Charge to 4.2V at 20A
2	Constant Voltage Charge to 0.06A at 4.2V
3	1 Hour Still (No Charge or Discharge)
4	Constant Current Discharge to 2.8V at 20A
5	1 Hour Still (No Charge or Discharge)

Table 2.2: Steps of a Single Cycle (Prismatic Cell)

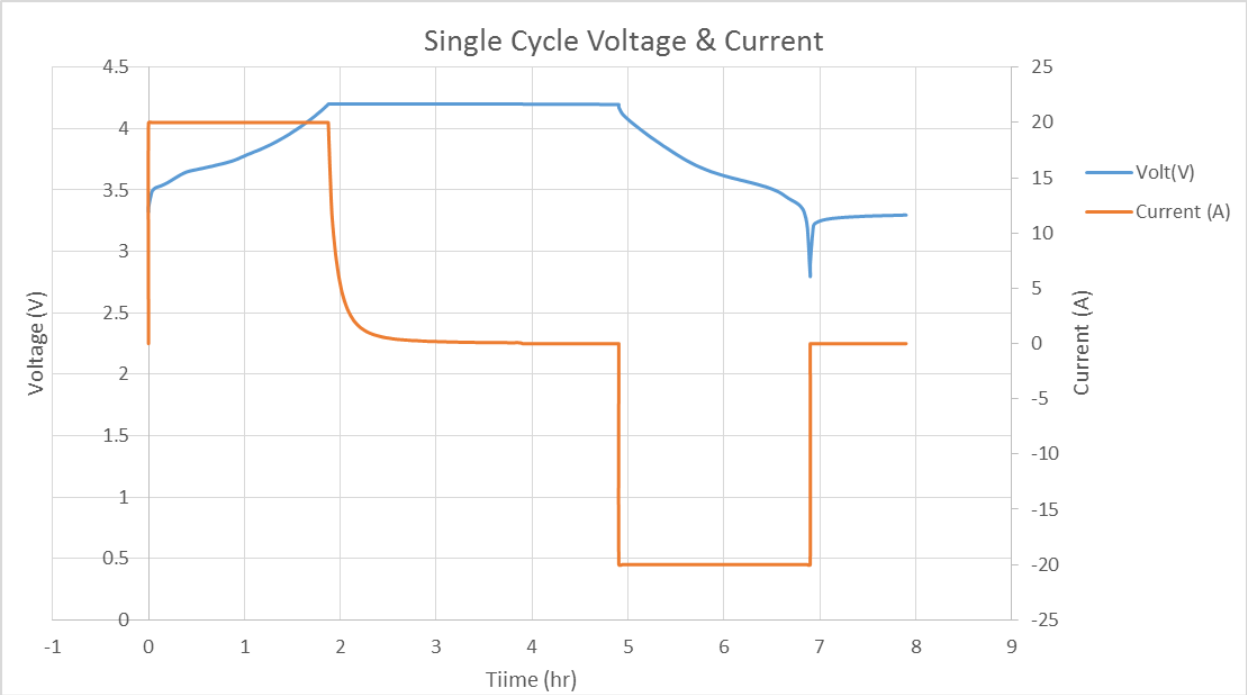

Figure 2-10: Voltage & Current Plot of a Single Cycle

20A was chosen because it represented the C/2 rate for the batteries, thus enabling the battery to be fully discharged in 2 hours. 0.06A was the minimum current the battery analyzer was capable of outputting. The 2.8V and 4.2V limits were chosen based on what was considered fully discharged and charged, respectively, for the batteries. Prior to any cycling, the battery analyzer was used to discharge the batteries to 2.8V and held still for 1 hour to remove any residual charge present. Batteries 1, 2, and 3 were cycled for 50, 20, and 10 cycles, respectively, at room temperature. The four different channels on the battery analyzer enabled the testing of up to four batteries simultaneously while each undergoes their own specific testing. In addition to the cycling, Battery 1 was subjected to a compression load throughout cycling via a 2 kN load cell on the Instron loading frame, shown in Figure 2-11.

Figure 2-11: Battery 1 Cycling Setup

The objective of using the Instron loading frame was to simulate a battery being constricted into a carriage, and measure the amount of force the battery would subject to its carriage while cycling throughout its lifetime. The Instron loading frame initially loaded Battery 1 with 100N upon completion of removing any residual charge present, and was maintained at a fixed displacement to measure the changes in force throughout the cycling of Battery 1.

The cycling of Batteries 1, 2, and 3 were staggered such that they all ended their cycling around the same time in order to help minimize any impact from calendar aging. This staggering

of cycling is also the reason why only Battery 1 was subjected to a compressive load during testing. Upon completion of the cycling, a still lasting at least 47 hours (for a total of at least 48 hours of still after the end of the final discharge) took place prior to indentation. Towards the end of this time period, Battery 4, which had been subjected to no cycling, had its residual charge removed prior to indentation. After the stills were complete, the batteries were individually indented to failure using the MTS loading frame and monitoring the voltage with the battery analyzer. Figure 2-12 shows the setup of Battery 1 prior to Indentation.

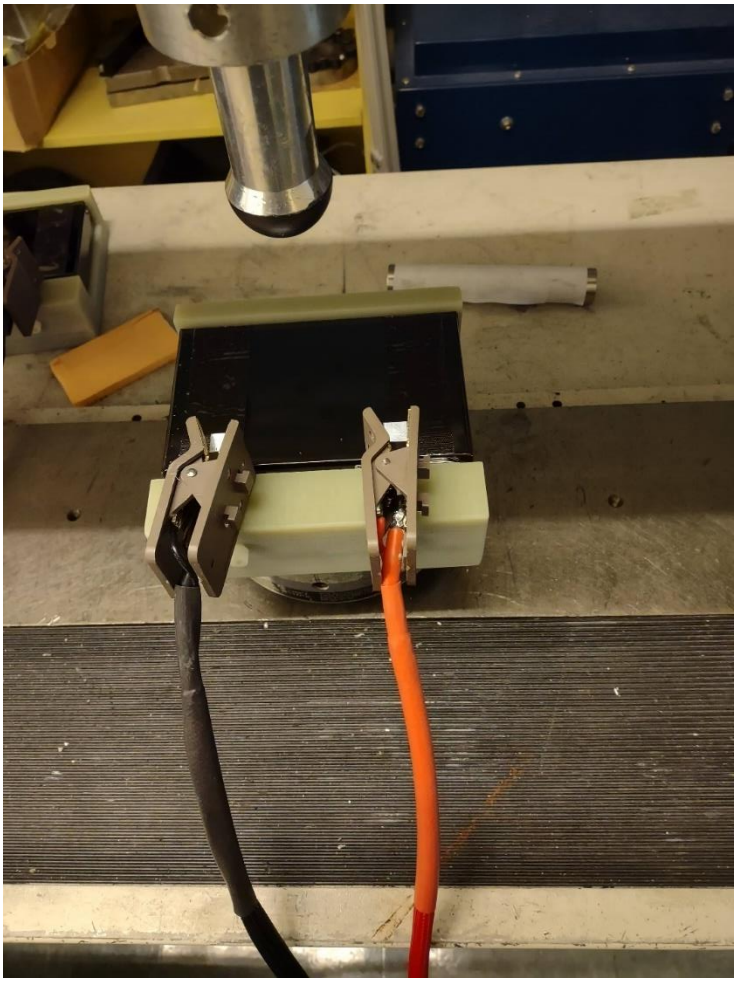

Figure 2-12: Battery 1 Indentation Set-Up

A 40 mm indenter attached to 200 kN load cell pressed down on the battery at a rate of 0.6 mm/min until it failed, indicated by a rapid decrease in the force applied by the MTS loading frame and the battery analyzer registering a voltage short in the battery. Table 2.3 summarizes the overall testing sequence for the prismatic cells:

Test Step #	Step Description
1	Battery 1 (50 Cycle) Residual Discharge begins
2	Battery 1 (50 Cycle) Residual Discharge ends Battery 1 (50 Cycle) Residual Still begins Battery 1 (50 Cycle) preloaded to 100N
3	Battery 1 (50 Cycle) Residual Still ends Battery 1 (50 Cycle) Cycling begins
4	Battery 2 (20 Cycle) Residual Discharge & Still begins
5	Battery 2 (20 Cycle) Residual Discharge & Still ends Battery 2 (20 Cycle) Cycling begins
6	Battery 3 (10 Cycle) Residual Discharge & Still begins
7	Battery 3 (10 Cycle) Residual Discharge & Still ends Battery 3 (10 Cycle) Cycling begins
8	Battery 2 (20 Cycle) Cycling ends Battery 2 (20 Cycle) Additional Still begins
9	Battery 1 (50 Cycle) Cycling ends Battery 1 (50 Cycle) Additional Still begins
10	Battery 3 (10 Cycle) Cycling ends Battery 3 (10 Cycle) Additional Still begins
11	Battery 2 (20 Cycle) Additional Still ends Battery 2 (20 Cycle) Indented
12	Battery 4 (0 Cycle) Residual Charge Removed Battery 4 (0 Cycle) Indented
13	Battery 1 (50 Cycle) Additional Still ends Battery 2 (50 Cycle) Indented
14	Battery 3 (10 Cycle) Additional Still ends Battery 2 (10 Cycle) Indented

Table 2.3: Summary of Overall Prismatic Cell Testing Sequence

2.3: Experiment Results & Conclusions

2.3.1: Cycling Results & Observations

Figure 2-13 shows the force measured by the Instron loading frame and the voltage measured by the battery analyzer as Battery 1 completed the 50 cycles of charging and discharging. Figure 2-14 shows the force and voltage measured for the first cycle of Battery 1. The plots show that the maximum force peaks correspond to transition from Constant Current to Constant Voltage charging, while the minimum force peaks correspond to the discharge periods of the battery. with the value of the peaks increasing as Battery 1 progressed through its cycles. Additionally, the maximum Force peaks gradually increased in value over the course of the cycling, going from about 110 N to about 250 N. Conversely, the minimum Force peaks stayed relatively constant at about 45 N.

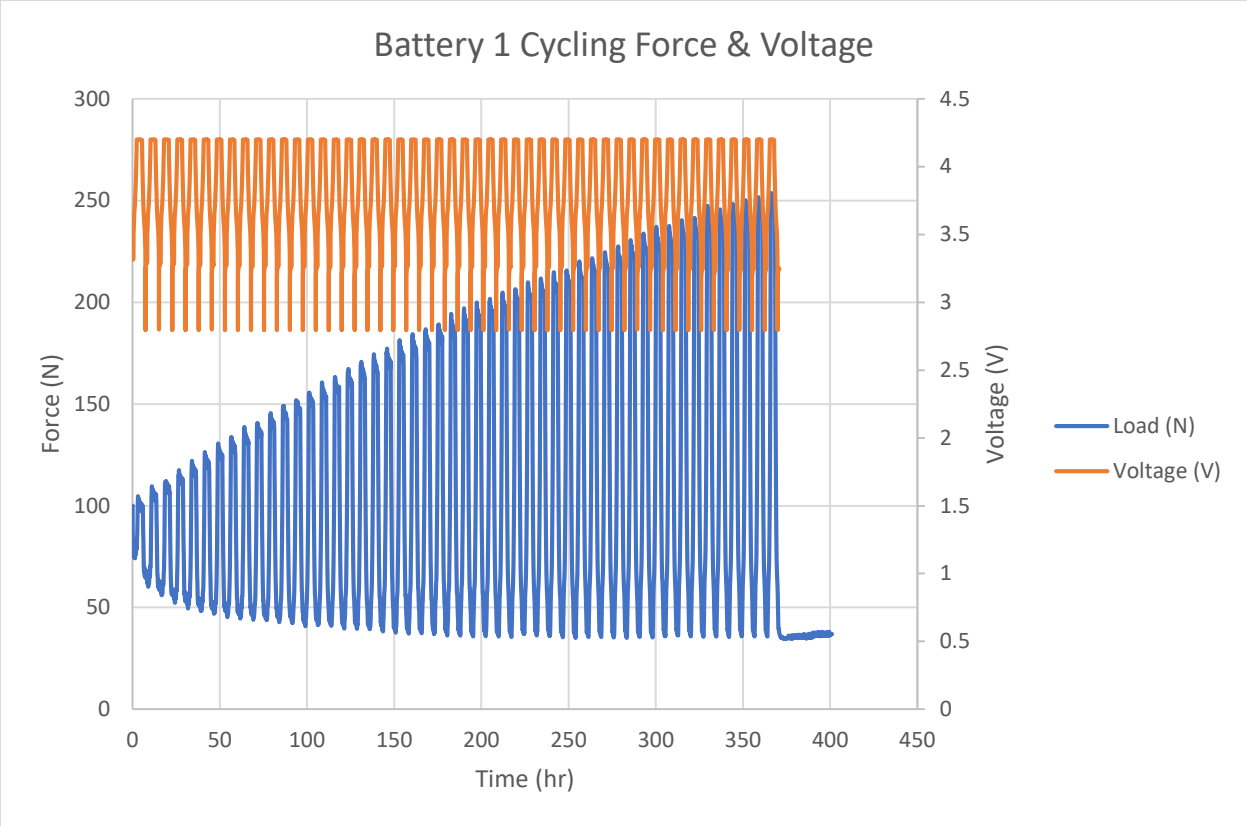

Figure 2-13: Voltage & Instron Force Over Time for Battery 1

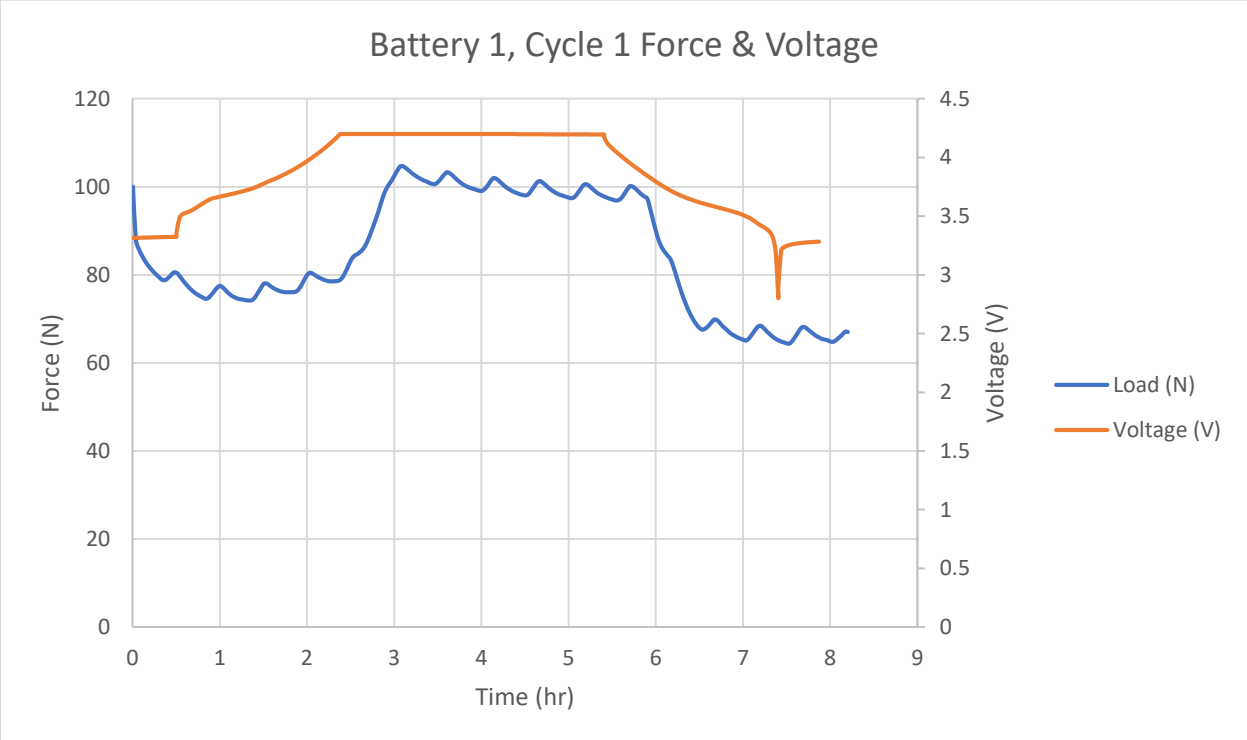

Figure 2-14: Voltage & Instron Force Over Time for 1st Cycle of Battery 1

Figure 2-15 shows the amount of time taken to charge Batteries 1, 2, and 3 as they progressed through their testing, while Figure 2-16 shows the amount of time taken to discharge the batteries. The charge time of Cycle 10 for Battery 2 is an outlier, due to a brief (< 1 minute) power interruption that occurred during testing. The impact on Battery 1 is not present in the charge times, despite it also charging during this power interruption. Battery 3 had not started testing yet, and thus was unaffected by the power interruption.

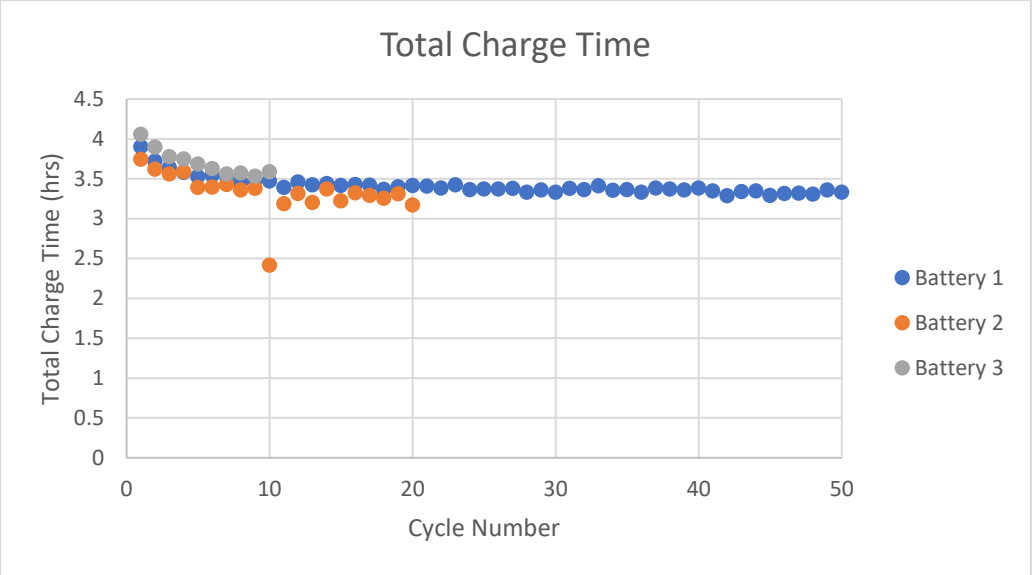

Figure 2-15: Prismatic Cell Charge Times

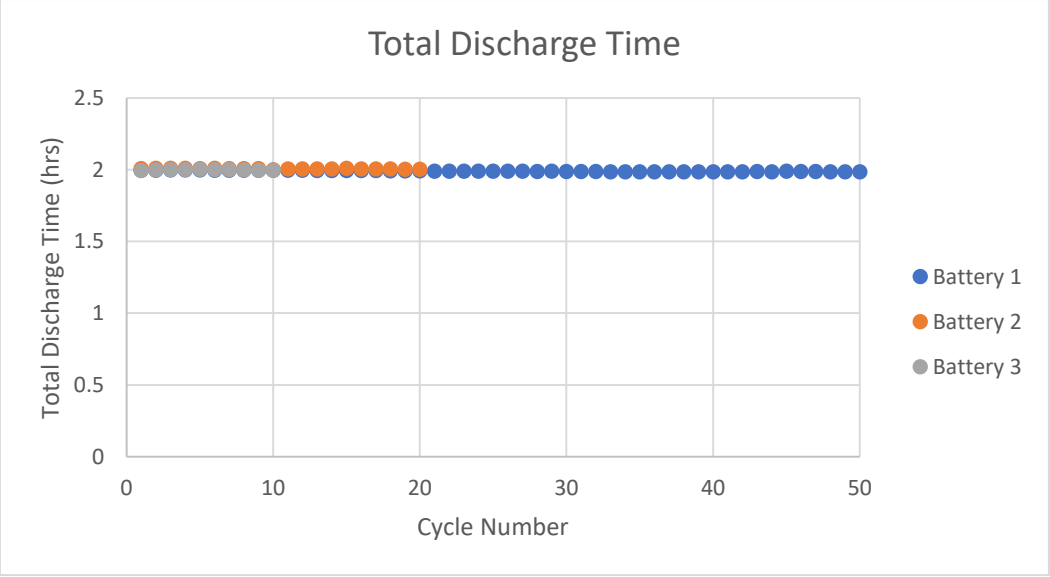

Figure 2-16: Prismatic Cell Discharge Times

The charge times for all three batteries show a similar trend of how they decreased from about 4 hours for the first cycle to about 3.5 hours for the 10th cycle. After the 10th cycle, the charge times for Batteries 1 and 2 show a slight decrease to about 3.3 and 3.2 hours, respectively. Conversely, the discharge times for all of the batteries were consistently about 2 hours long.

Figure 2-17 and Figure 2-18 show all of the charge and discharge capacities, respectively, of the batteries as they progressed through their testing. The impact previously mentioned power interruption on the charge and discharge capacities of Cycle 40 for Battery 1 and of Cycle 10 for Battery 2 are only clearly seen when zooming in on the data in Figure 2-19 and Figure 2-20. All of the capacities, charge and discharge, decreased in the same manner for all three batteries from their respective first and final cycles.

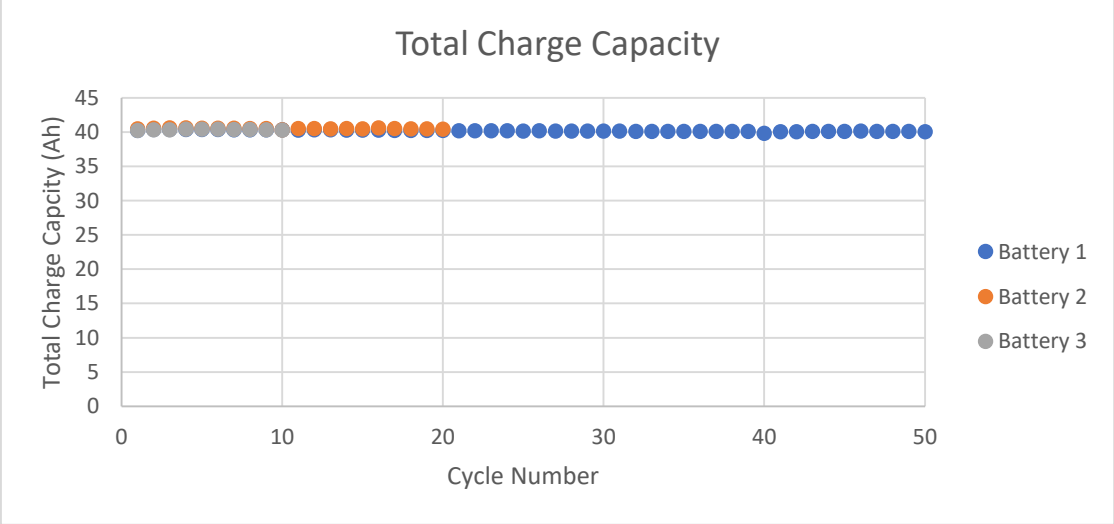

Figure 2-17: Prismatic Cell Charge Capacities

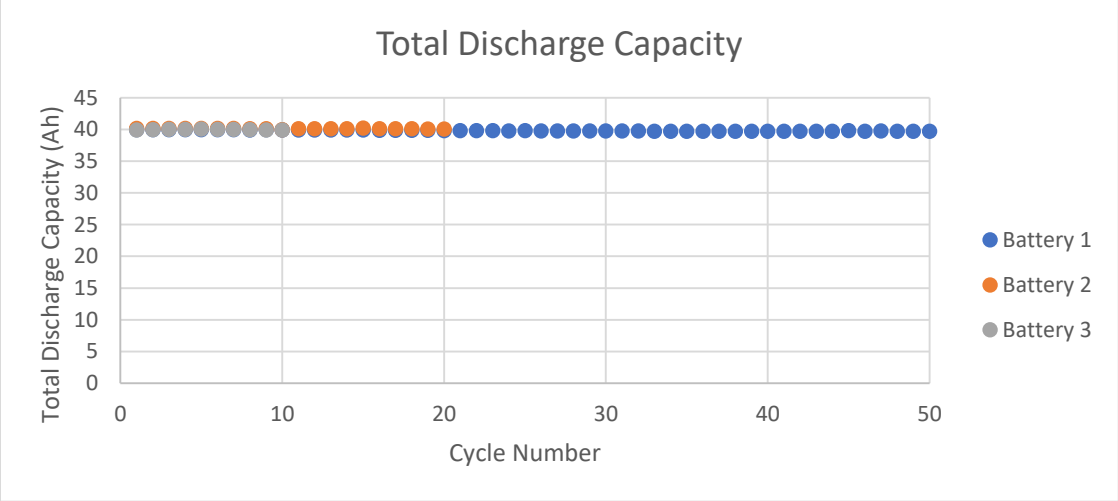

Figure 2-18: Prismatic Cell Discharge Capacities

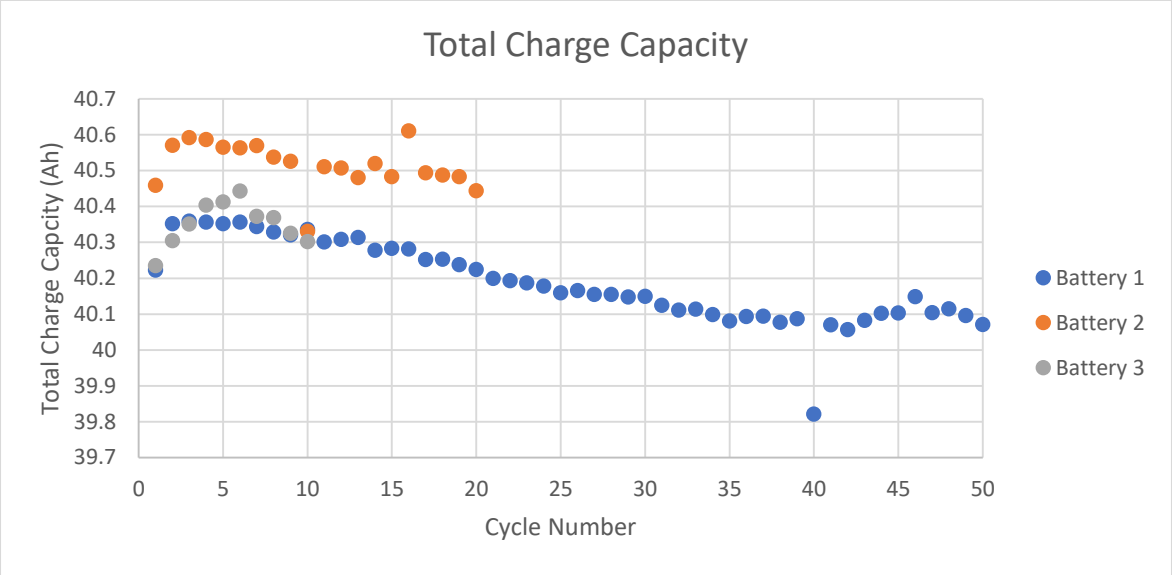

Figure 2-19: Prismatic Cell Charge Capacities (Zoomed In)

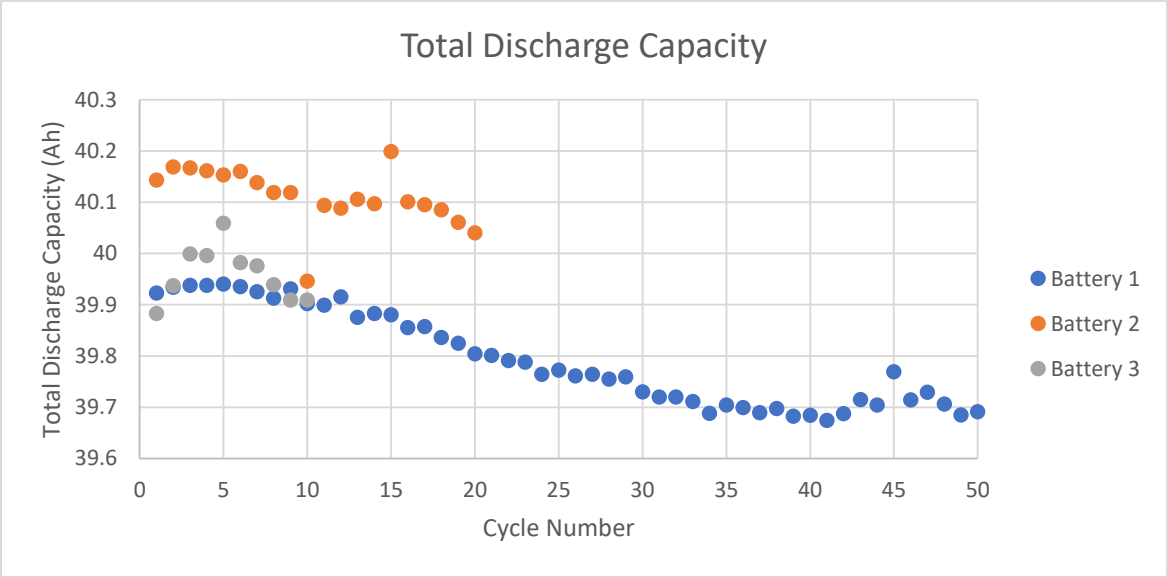

Figure 2-20: Prismatic Cell Discharge Capacities (Zoomed In)

When considering the time lengths and capacities together, one additional observation can be made about the prismatic cells. The first 10 cycles (during which the charge times quickly decayed) of all three batteries had cumulative charge and discharge capacitates of approximately 400 Ah. After 400 Ah have been charged and discharged out of the battery, the charge times proceeded to decay much slower.

2.3.2: Indentation Results & Observations

Figure 2-21 shows all Force-Displacement curves for the batteries, while Figure 2-22 through Figure 2-25 show the damage done to the batteries via the indentation.

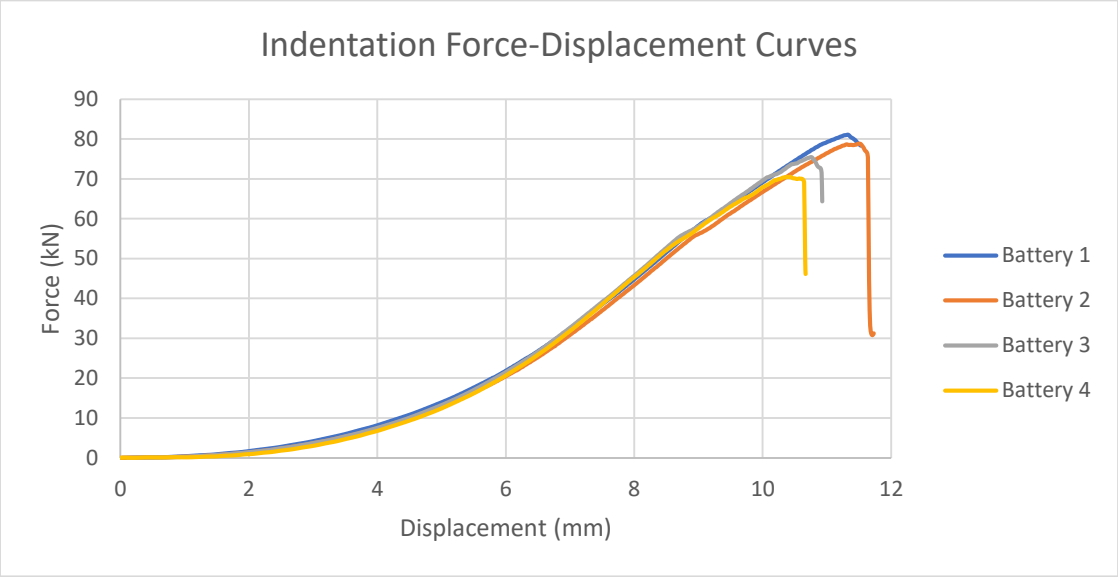

Figure 2-21: Indentation Force-Displacement Curves

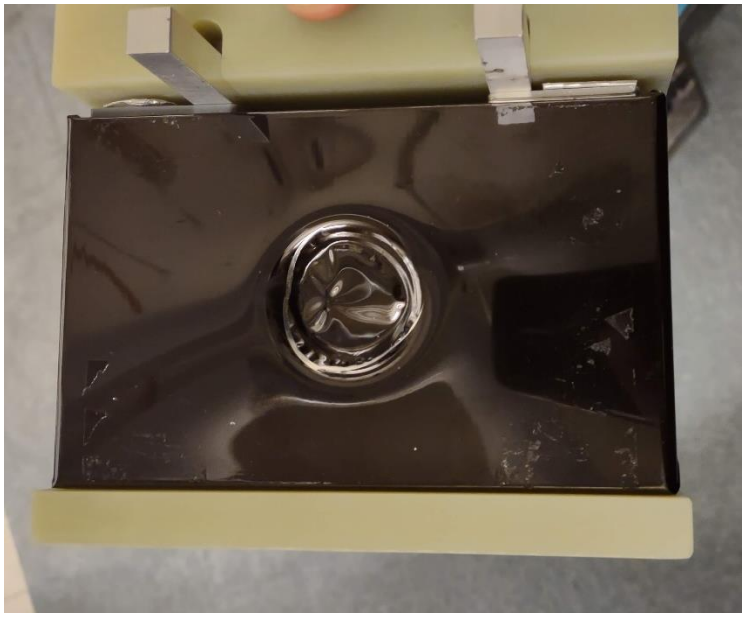

Figure 2-22: Battery 1 Post Indentation

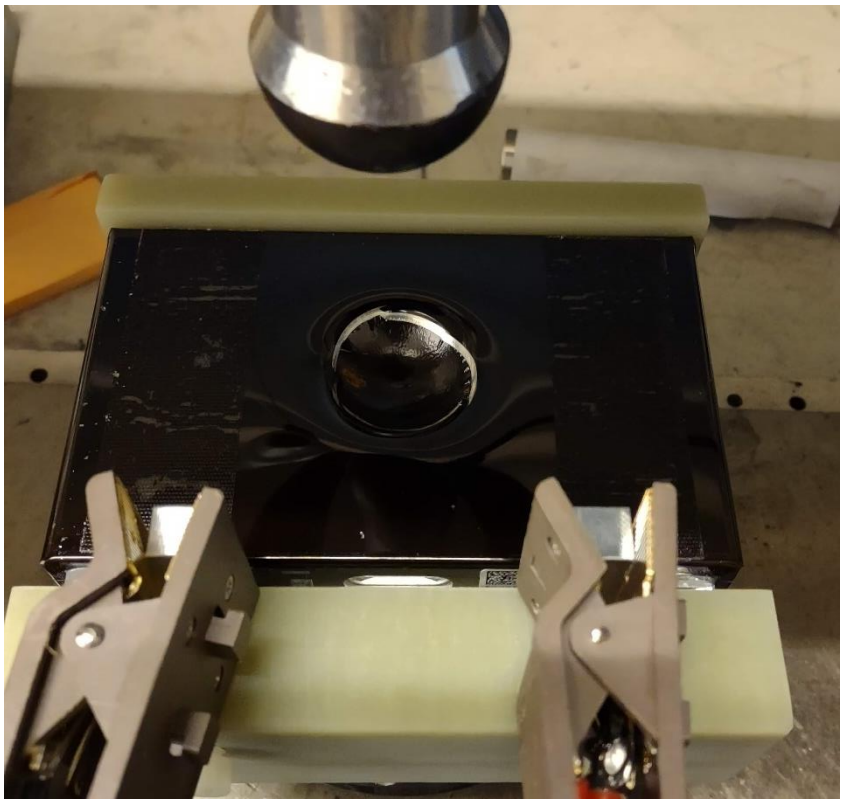

Figure 2-23: Battery 2 Post Indentation

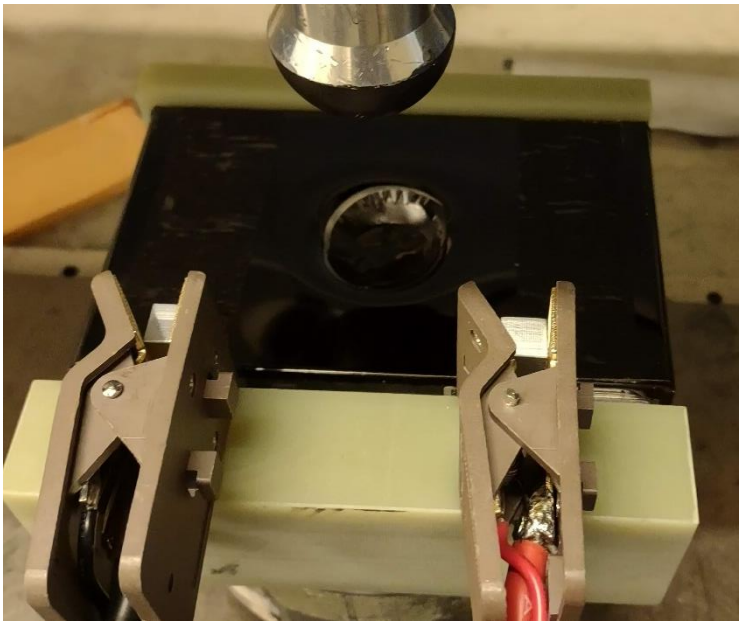

Figure 2-24: Battery 3 Post Indentation

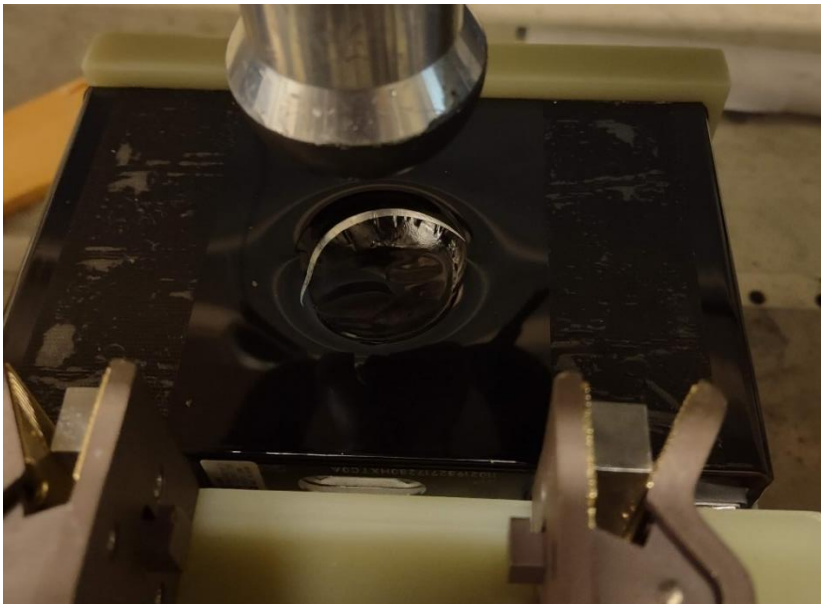

Figure 2-25: Battery 4 Post Indentation

While the amount of time to break each battery varied, what is clear is that the more the battery was cycled, the more force that was required to break it. Additionally, despite the difference in required force to break the battery, all four of them failed at after a similar amount of indentation. Table 2.4 lists the peak indentation force and failure displacement experienced by each battery, and Figure 2-26 plots the peak indentation force versus the number of cycles.

Battery #	# of Cycles	Peak Force (kN)	Failure Displacement (mm)
1	50	81.086	11.333
2	20	78.814	11.494
3	10	75.481	10.759
4	0	70.458	10.423

Table 2.4: Peak Indentation Force & Failure Displacement

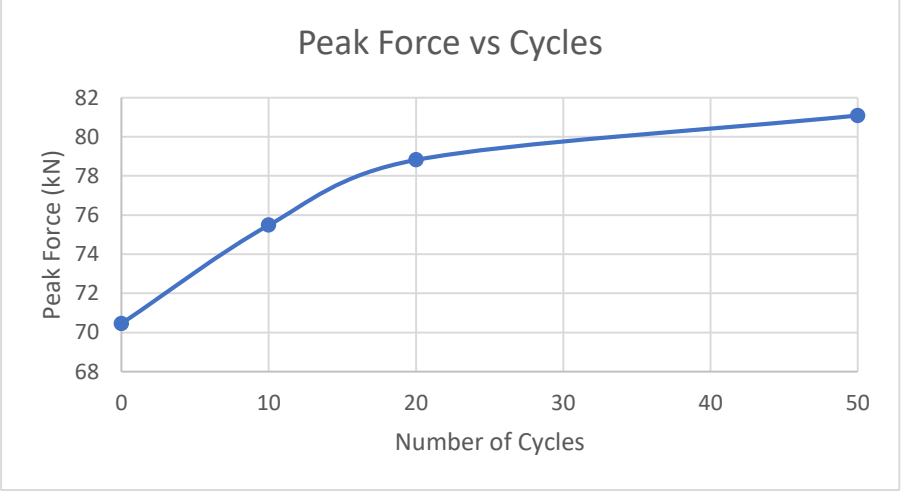

Figure 2-26: Peak Indentation Force vs. Cycles

Chapter 3: Pouch Cell Four-Point Bending

3.1: Pouch Cell & Experimental Description

Six pouch type lithium ion cells, pictured in Figure 3-1, were used for this study. Table 3.1 list the relevant properties of the cells. These pouch cells, from a used Nissan Leaf Electric Vehicle, were much older than the prismatic cells that were used in the previous experiment.

Figure 3-1: Lithium-Ion Pouch Cell

Property	Value
Nominal Capacity	25Ah
Nominal Voltage	3.5V
Width	15 mm
Length	195 mm
Thickness	7.6 mm

Table 3.1: Lithium-Ion Pouch Cell Properties

The battery analyzer used for the prismatic cells was also utilized to cycle the pouch cells. As only one pouch cell could be used on the MTS loading frame at a time, they were testing in series vice parallel as the prismatic cells were. Each pouch cell had its residual charge removed and 30 minutes later were deflected by 10 mm using the MTS loading frame and its 200 kN loading cell. The pouch cell was cycled 10 times while remaining under constant deflection.

Table 3.2 summarizes the testing completed on the pouch cells. The first distance listed corresponds to which fixed indenter was used, and will be used to label the pairs of cells tested.

Top Indenter Distance	Bottom Support Distance	Pouch Cells Tested
60 mm	95 mm	1, 2
90 mm	145 mm	3, 4
120 mm	195 mm	5, 6

Table 3.2: Four-Point Bending Test Summary

3.2: Experiment Setup & Method

3.2.1: Bending Rig Development

Three fixed distance indenters and two moveable bottom supports were designed and built in order to accomplish the four-point bending. Figure 3-2 through Figure 3-5 show the schematics of these individual parts, while Figure 3-6 shows an example of how the pieces fit together.

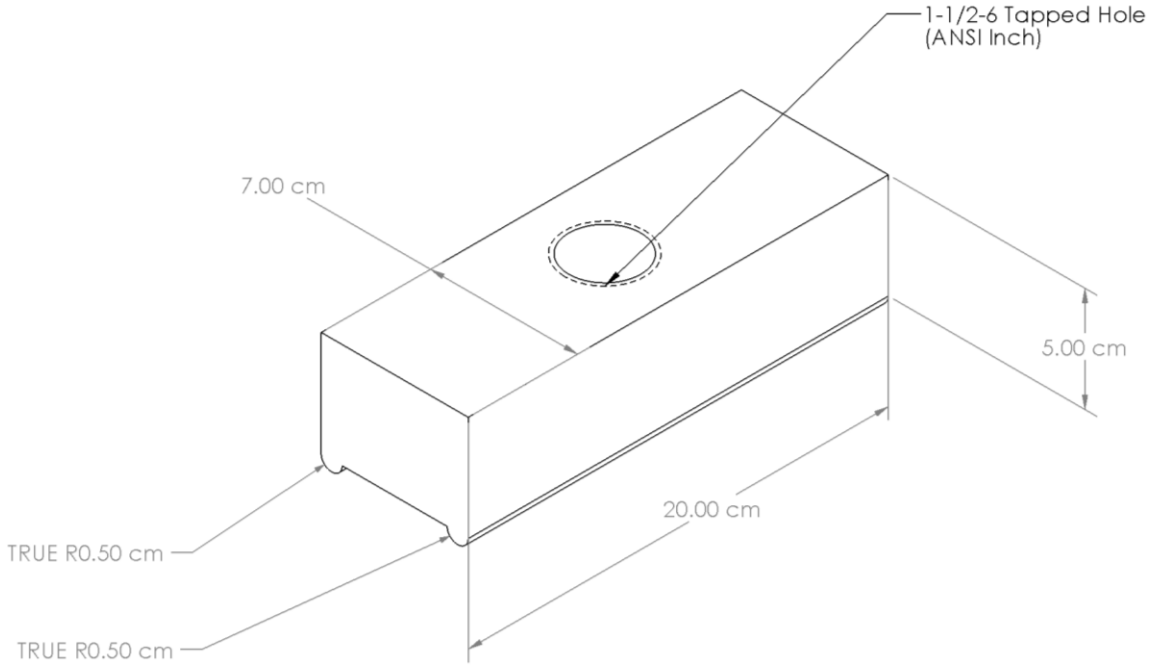

Figure 3-2: 60 mm Indenter

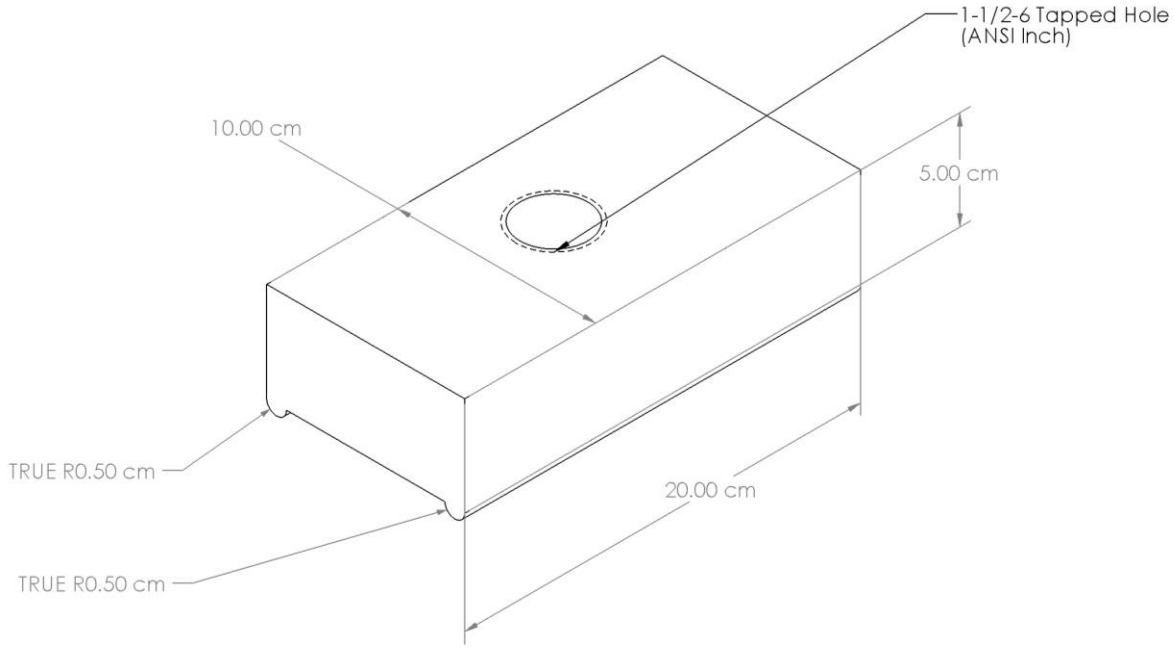

Figure 3-3: 90 mm Indenter

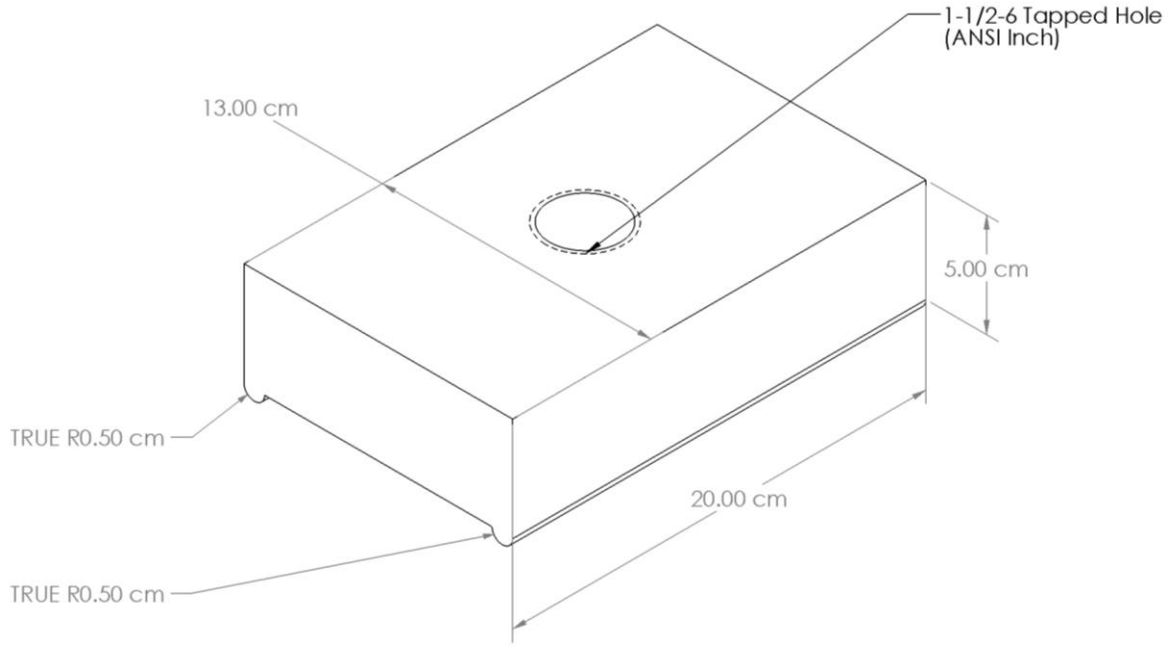

Figure 3-4: 120 mm Indenter

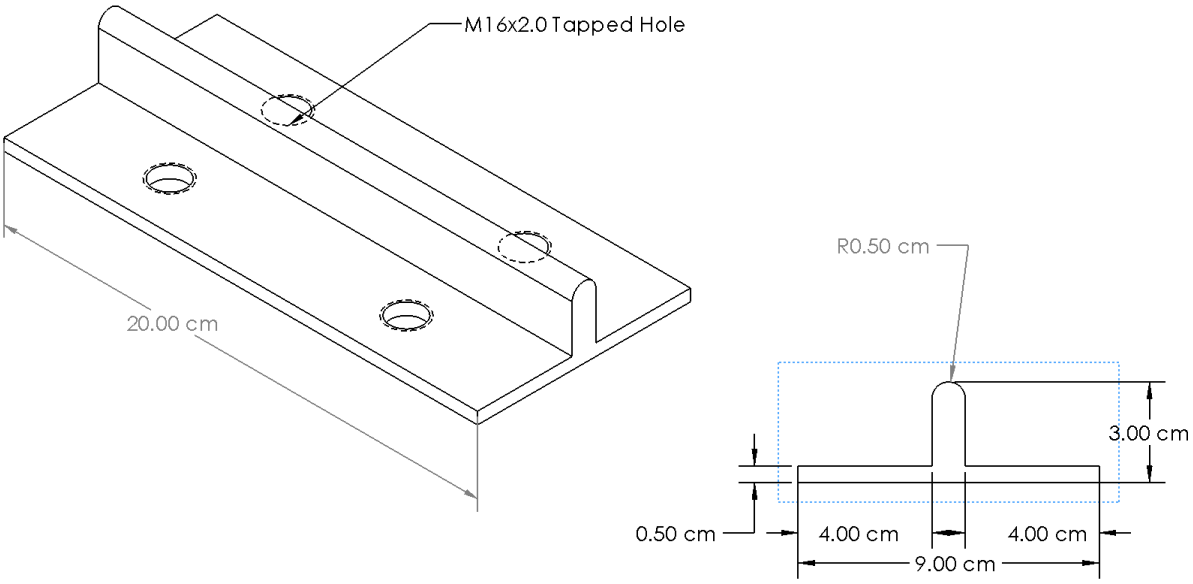

Figure 3-5: Moveable Bottom Support

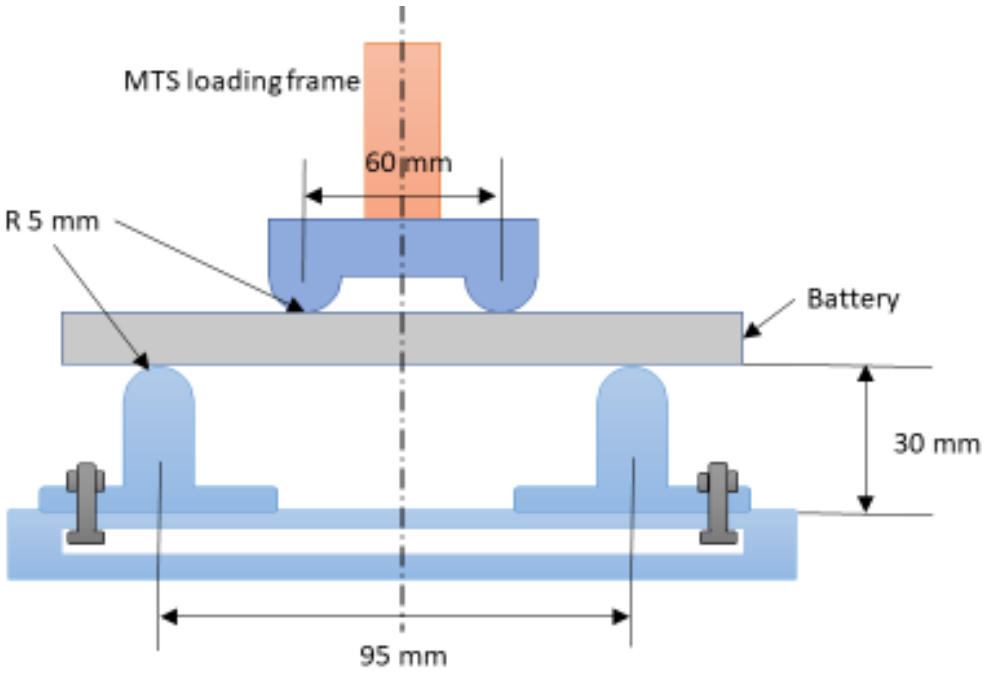

Figure 3-6: Example Schematic

(Note: The bottom supports bolted into a plate previously used in other ICL experiments)

3.2.2: Experiment Procedure

The six pouch cells were tested one at a time using the battery analyzer and MTS loading frame. The moveable bottom supports were set to the appropriate distance, and the appropriate top

indenter was attached to the 200 kN loading cell of the MTS loading frame. The battery analyzer was used to discharge the cell to 2.8V prior to any cycling to remove any residual charge present, and then hold still for 1 hour prior to commencing the cycling. Figure 3-7 shows the setup for Pouch Cell 1 prior to bending.

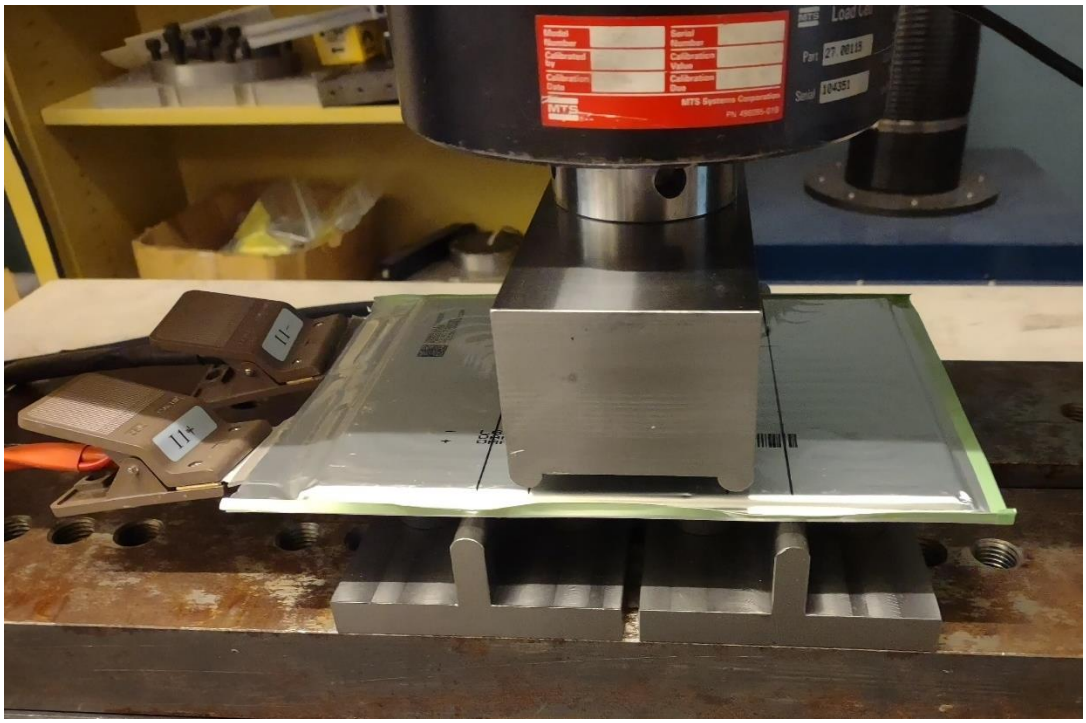

Figure 3-7: Pouch Cell 1 Bending Setup

Halfway into the still, the MTS loading frame bent the pouch cell at a rate of 6 mm/min until reaching 10 mm of displacement. Upon completion of the bending, each pouch cell underwent 10 cycles, with a single cycle consisting of the steps listed in Table 3.3:

Cycle Step #	Cycle Step
1	Constant Current Charge to 4.2V at 12.5A
2	Constant Voltage Charge to 0.06A at 4.2V
3	1 Hour Still (No Charge or Discharge)
4	Constant Current Discharge to 2.8V at 12.5A
5	1 Hour Still (No Charge or Discharge)

Table 3.3: Steps of a Single Cycle (Pouch Cell)

The only difference between the pouch cell and prismatic cell cycles was the maximum current used, as the pouch cells had a lower capacity than the prismatic cells. Thus, the pouch cells used a maximum current of 12.5A as opposed to the 20A of the prismatic cells. During the final still (corresponding to the 10^{th} cycle), the indenter was raised off the pouch cell. The pouch cell was

removed from the MTS loading frame, and if necessary for the next pouch cell the indenter was swapped and the bottom supports moved. The testing sequence, summarized in Table 3.4, was repeated until all six pouch cells had been tested.

Test Step #	Step Description
1 (as necessary)	Appropriate Top Indenter installed Bottom Supports set to appropriate distance
2	Residual Discharge performed
3	Residual Still Begin
4	30 minutes into Residual Still: pouch cell bent
5	Residual Still ends Cycling begins
6	30 minutes into still of 10^{th} cycle: Top Indenter raised
7	Cycling ends
8 (as necessary)	Preparation for next pouch cell test

Table 3.4: Summary of Single Pouch Cell Testing Sequence

Upon completion of the cycling, one cell from each pair was selected to cut in half in order to inspect the internals of the cell post bending. These cells were discharged at 6.25A, corresponding to the C/4 rate, to their cutoff voltage of 2V in order to remove any residual charge present prior to cutting them inside of a fume hood.

3.3: Experiment Results & Conclusions

3.3.1: Deflection Results & Observations

Figure 3-8 through Figure 3-10 show the Force-Displacement curves for each bending distance, and Figure 3-11 shows all Force-Displacement curves on a single chart. Figure 3-12, Figure 3-13, and Figure 3-14 show a pouch cell on the MTS loading frame for 60 mm, 90 mm, and 120 mm, respectively. Table 3.5 details the peak bending force. Figure 3-15 shows the voltage of all the pouch cells as the bending occurred during the residual still.

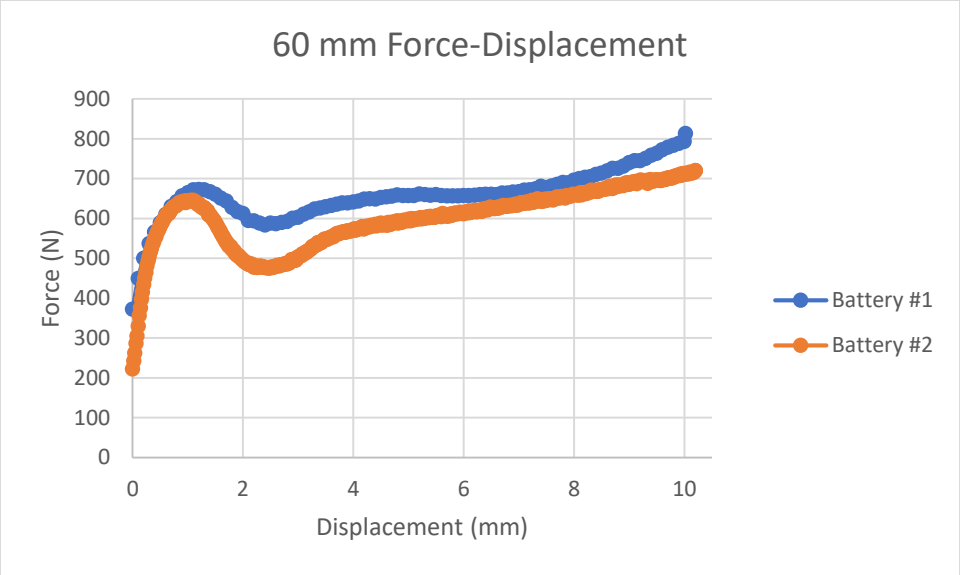

Figure 3-8: 60 mm Force-Displacement Curves

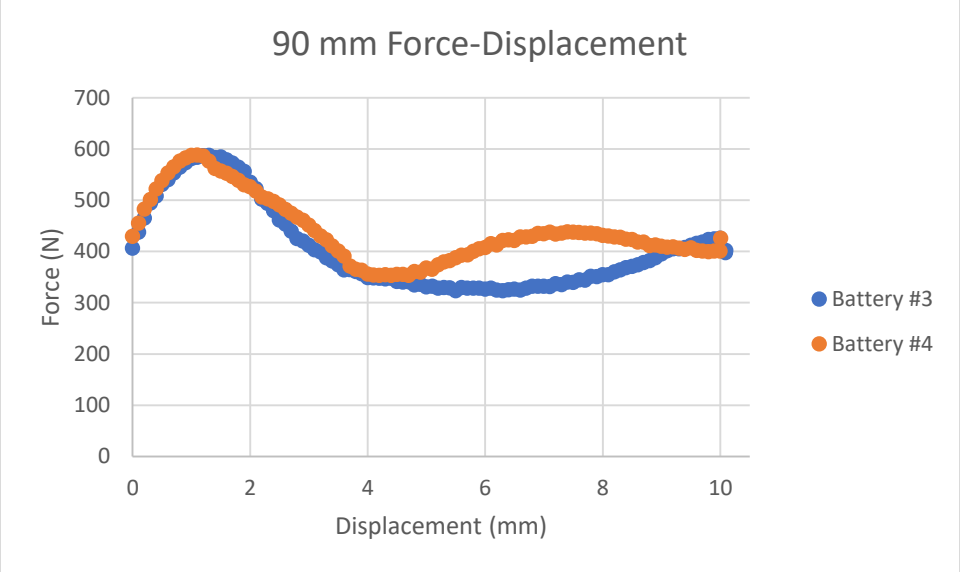

Figure 3-9: 90 mm Force-Displacement Curves

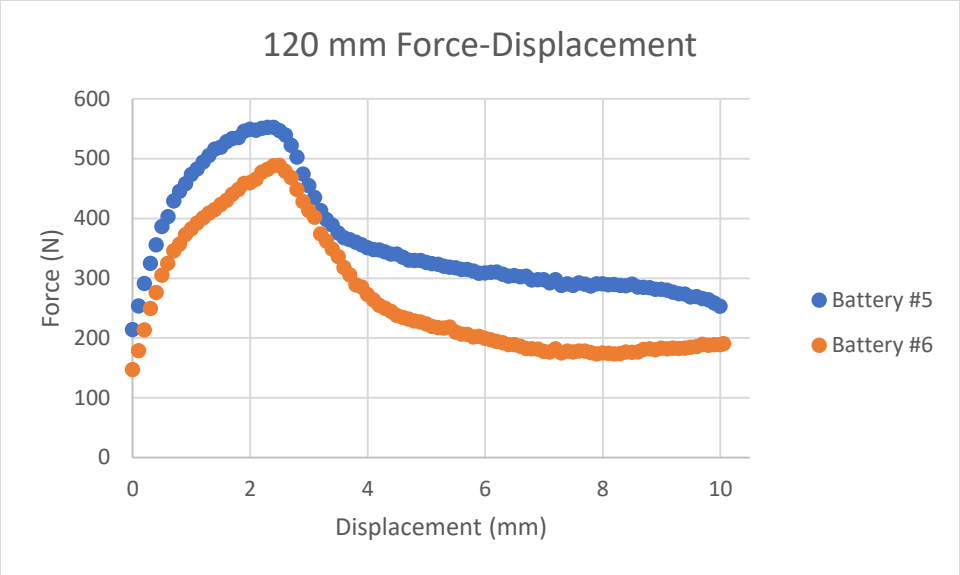

Figure 3-10: 120 mm Force-Displacement Curves

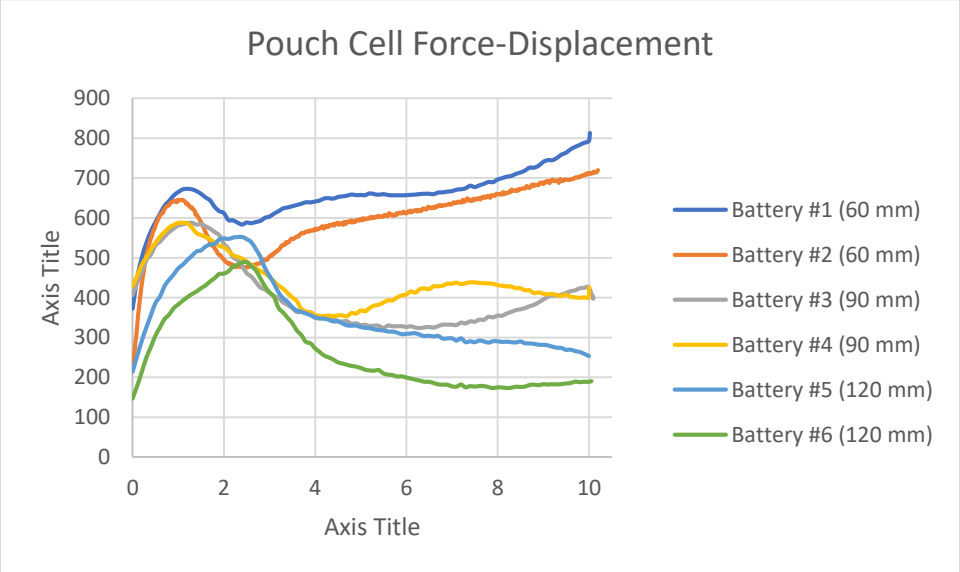

Figure 3-11: All Force-Displacement Curves

Figure 3-12: Battery 1 Indentation

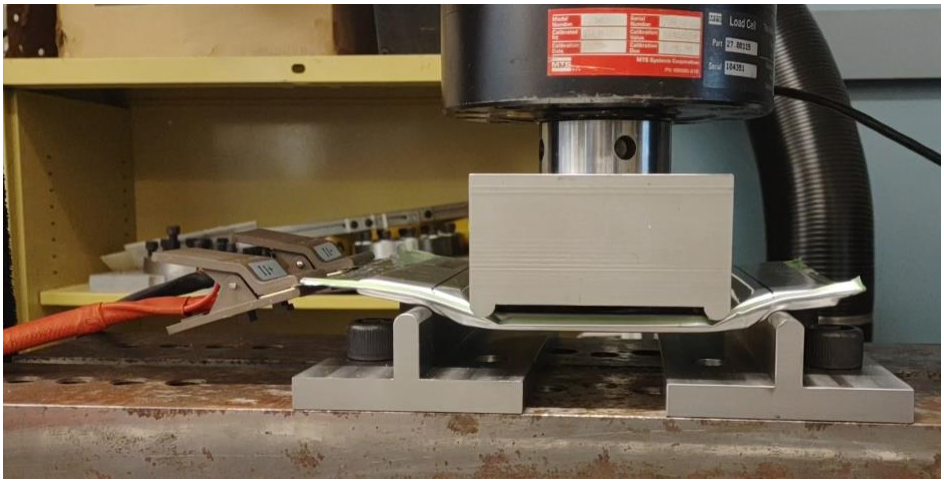

Figure 3-13: Battery 3 Indentation

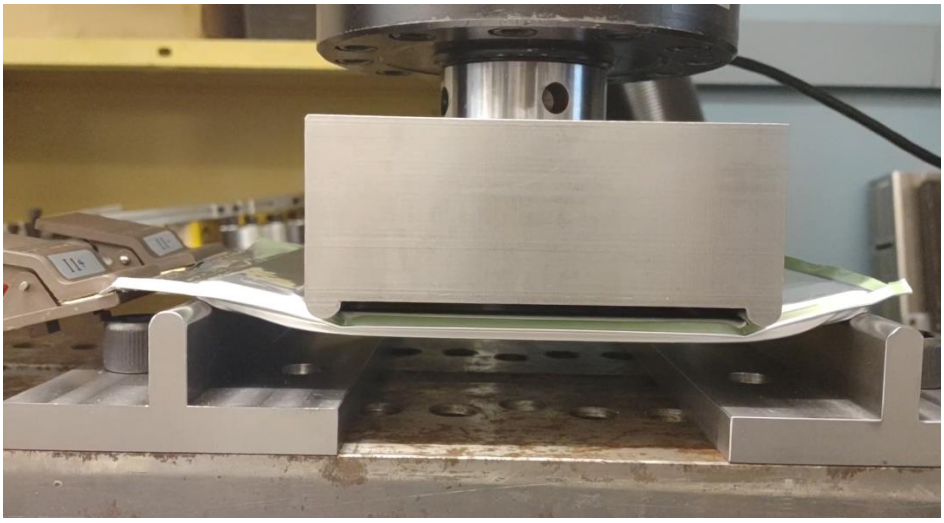

Figure 3-14: Battery 5 Indentation

Pouch Cell #	Peak Bending Force (kN)
1	813.429
2	645.532
3	587.587
4	588.3
5	552.483
6	488.604

Table 3.5: Peak Bending Force

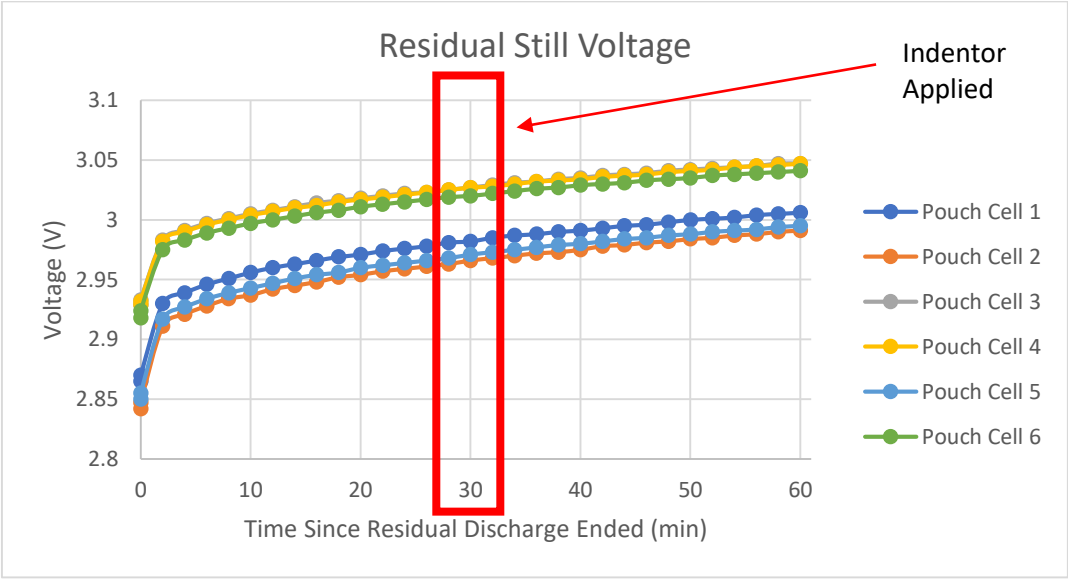

Figure 3-15: Residual Still Voltage

Figure 3-15 clearly shows that no short circuit occurred in any of the cells during the bending process. Conversely, several interesting observations come from the Force-Displacement curves.

The 60 mm indenter (which was the narrowest) had the largest bending forces, while the 120 mm indenter (which was the widest) had the smallest bending forces. Even though these two indenters had large differences in their peak bending forces, they produced Force-Displacement curves that had similar shapes across pouch cells. The 60 mm indenter reached its peak bending force at about 1 mm, at which point the force started reducing until about 2.25 mm. At that point, the bending force reaches a local minimum, and then proceeds to steadily increase until reaching 10 mm of displacement. Pouch cell 1 had a local minimum of 583.344 kN, while pouch cell 2 had a local minimum of 475.389 kN. The 120 mm indenter reached its peak bending force around the 2.25 mm point, after which the bending force decreases in a parabolic manner for about an additional 1 mm. At this 3.75 mm point, the shape of the curve smooths out, decreasing in a more linearly rate.

The 90 mm indenter differed from the other two in that that the peak bending forces for pouch cells 3 and 4 were within 1 kN of each other, but the Force-Displacement curves don't have similar shapes. Both pouch cells 3 and 4 reach their peak bending force around 1 mm. However, after this point, the pouch cell 3 Force-Displacement curve resembles the 120 mm indenter curves, in that the bending force decreases in a parabolic manner and then smooths out, and eventually starts to increase again. Pouch cell 4 Force-Displacement curve lightly resembles the 60 mm indenter curves, in that it decreases to a local minimum of 353.035 kN near 4 mm, increases to a local maximum of 438.348 kN near 7 mm, and then decreases again as displacement approaches 10 mm.

3.3.2: Cycling Results & Observations

Figure 3-16 and Figure 3-17 show the amount of time taken to charge and discharge, respectively, the pouch cells as they progressed through their testing. Figure 3-18 and Figure 3-19 show the charge and discharge capacities, respectively, of the pouch cells.

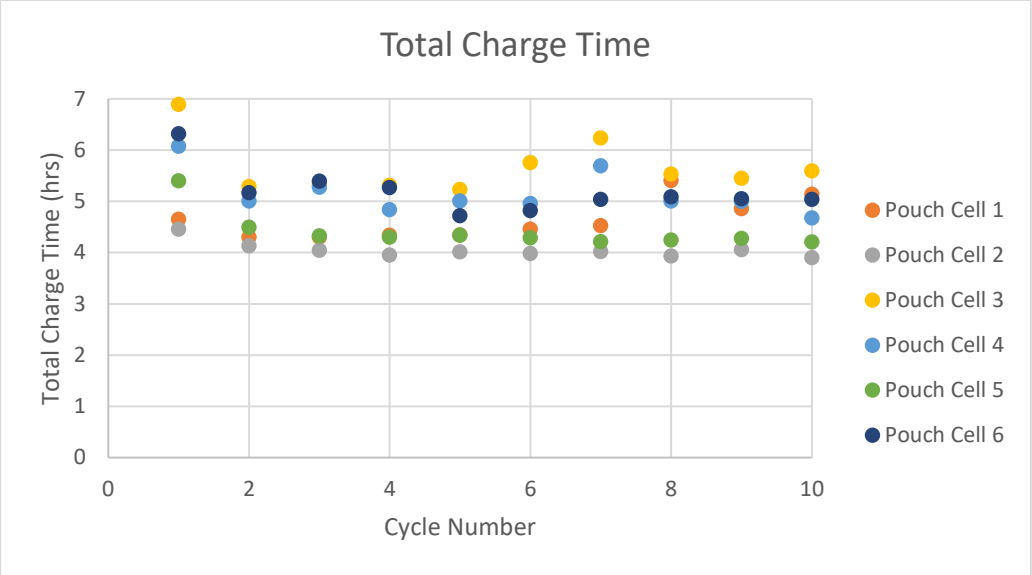

Figure 3-16: Pouch Cell Charge Times

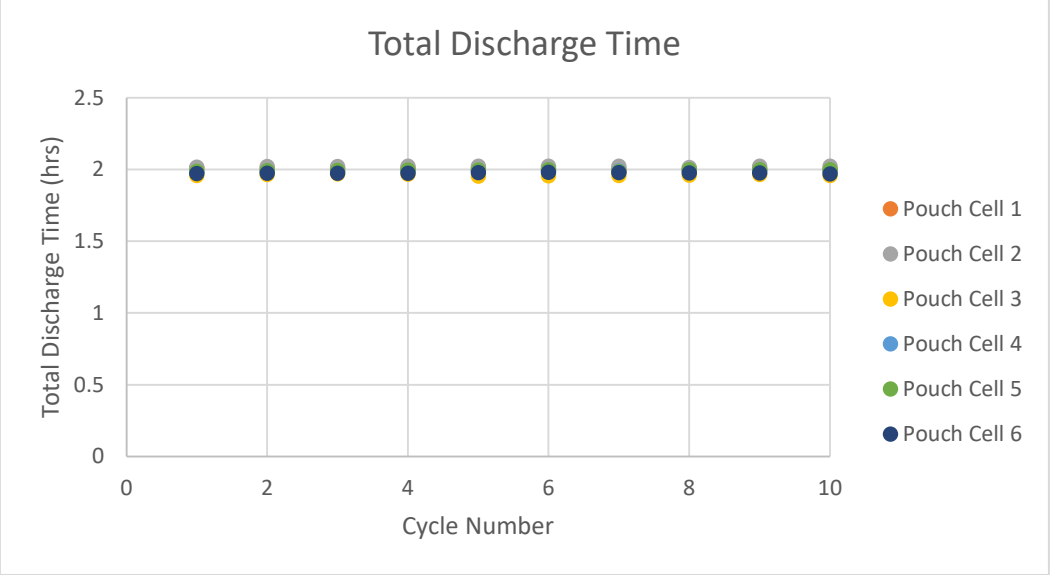

Figure 3-17: Pouch Cell Discharge Times

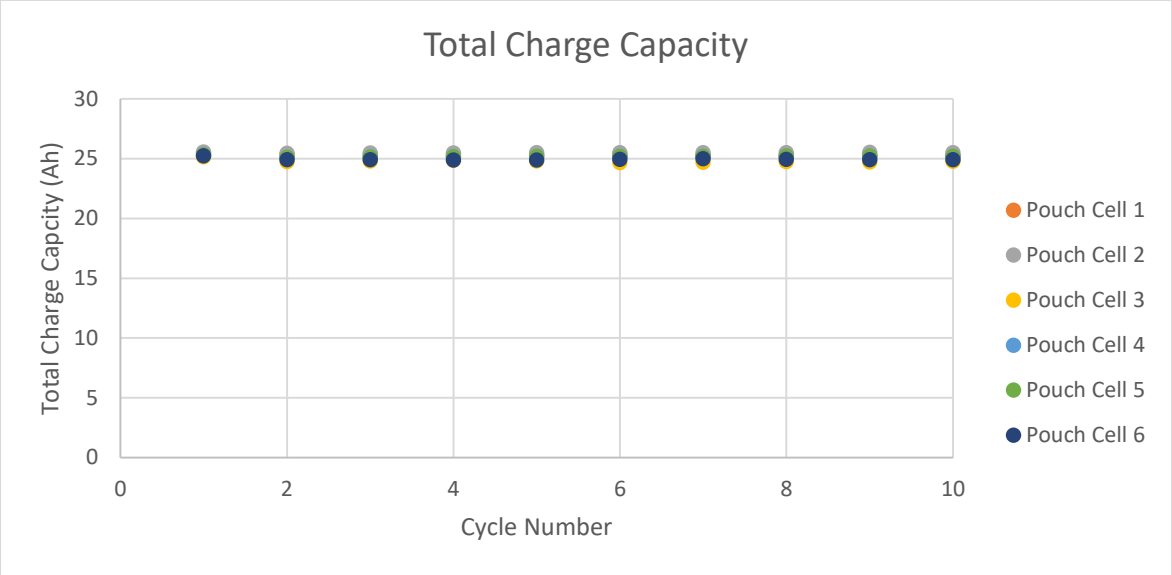

Figure 3-18: Pouch Cell Charge Capacities

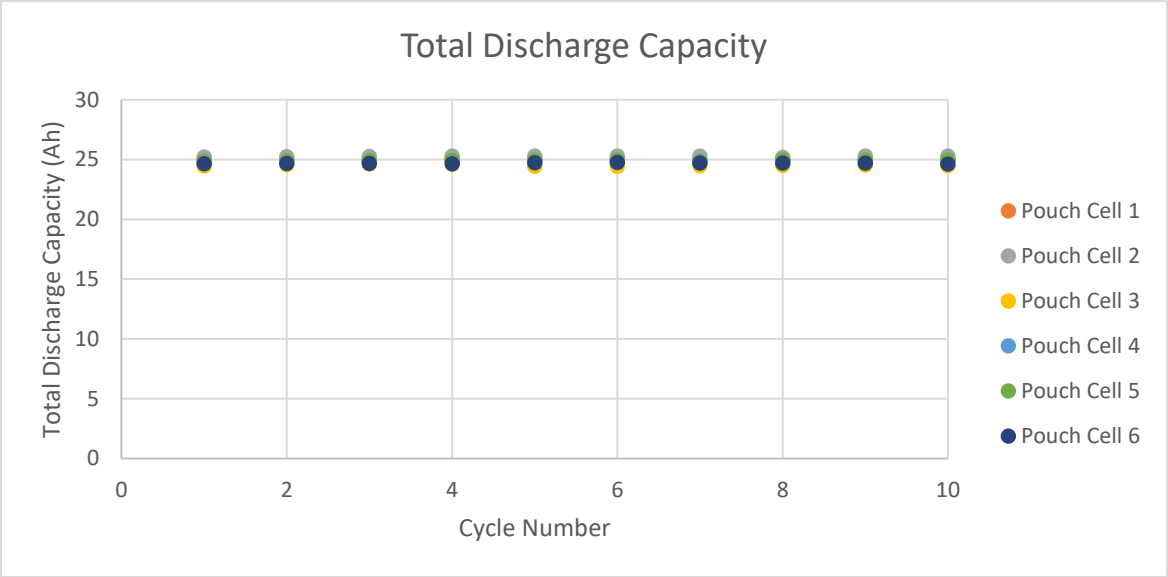

Figure 3-19: Pouch Cell Discharge Capacities

The charge times widely vary both within indenter pairs and across all six pouch cells. This is most likely due to age of the cells. Despite this large variation in charge times, all of the pouch cells discharged for approximately 2 hours with little variation, and had similar charge and discharge capacities.

Figure 3-20 through Figure 3-22 show the force measured by the MTS loading frame while the pouch cells went through their cycles, separated by top indenter distance. Similar to the Battery 1 of the prismatic cells, the maximum force peaks correspond to the transition from Constant

Current to Constant Voltage charging, and the minimum force peaks correspond to the discharge periods.

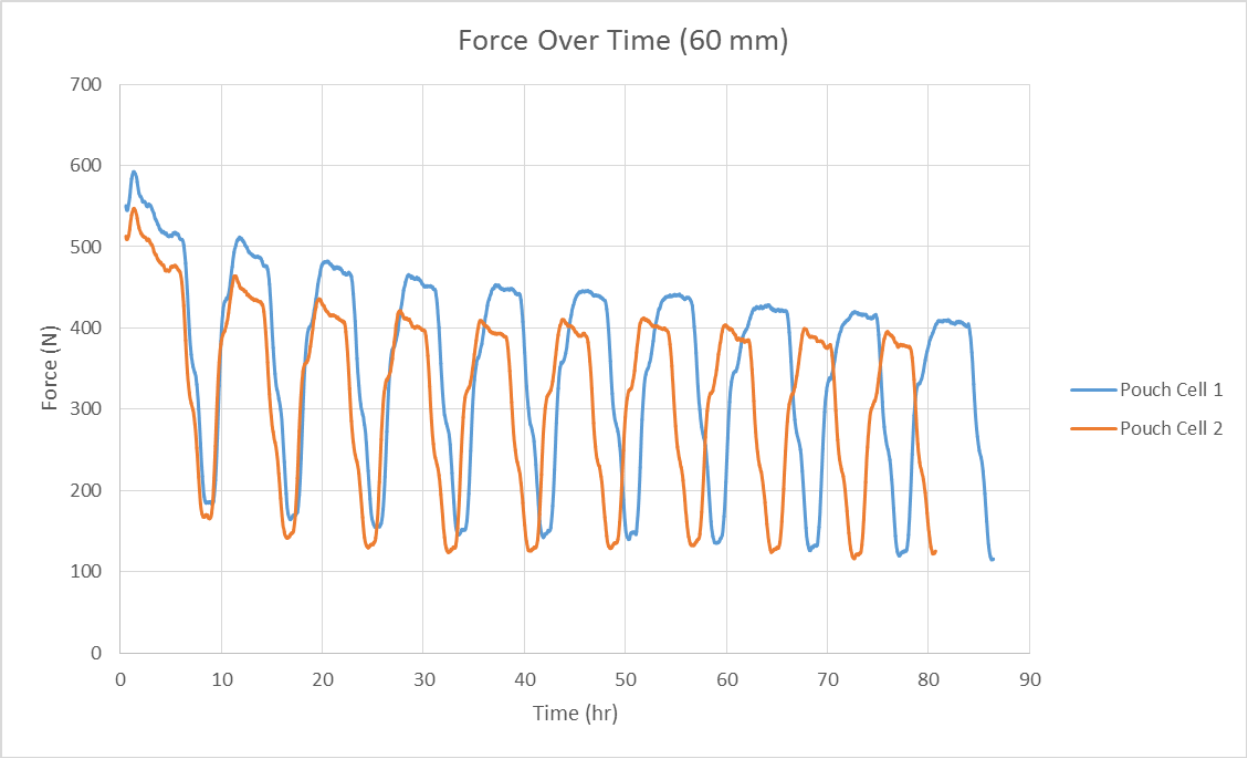

Figure 3-20: 60 mm Force over Time Curves

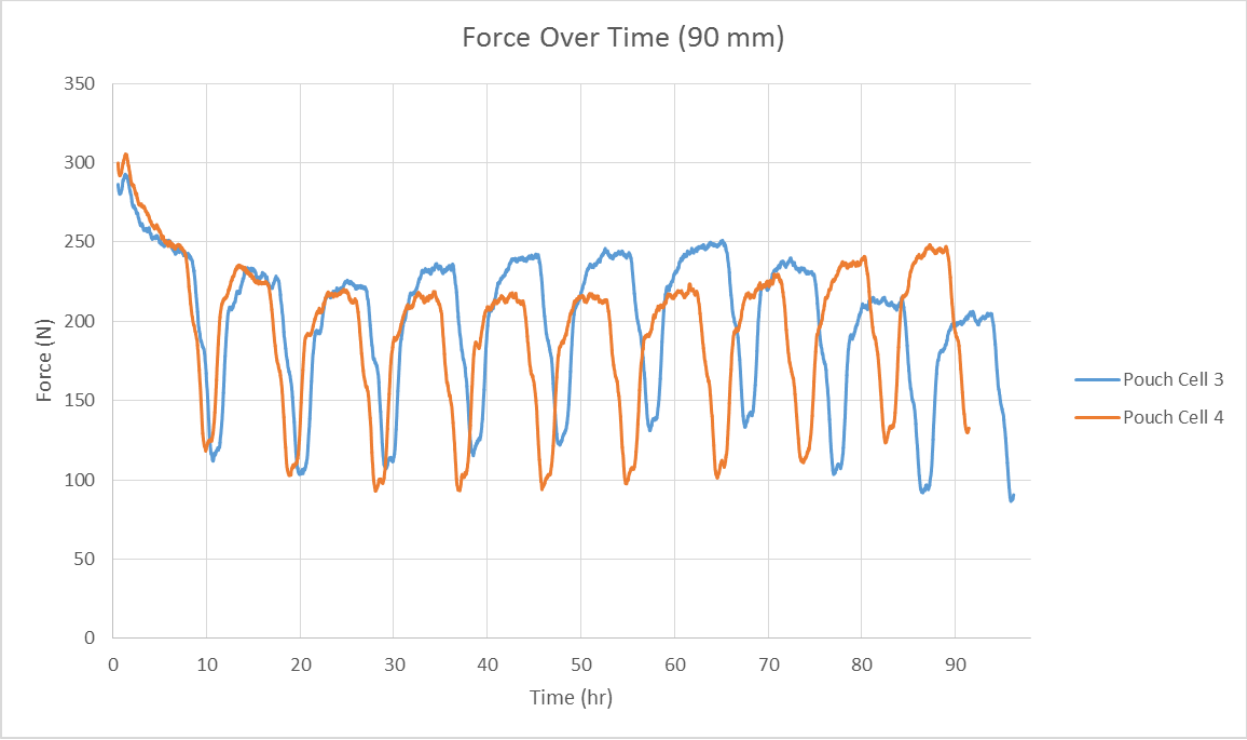

Figure 3-21: 90 mm Force over Time Curves

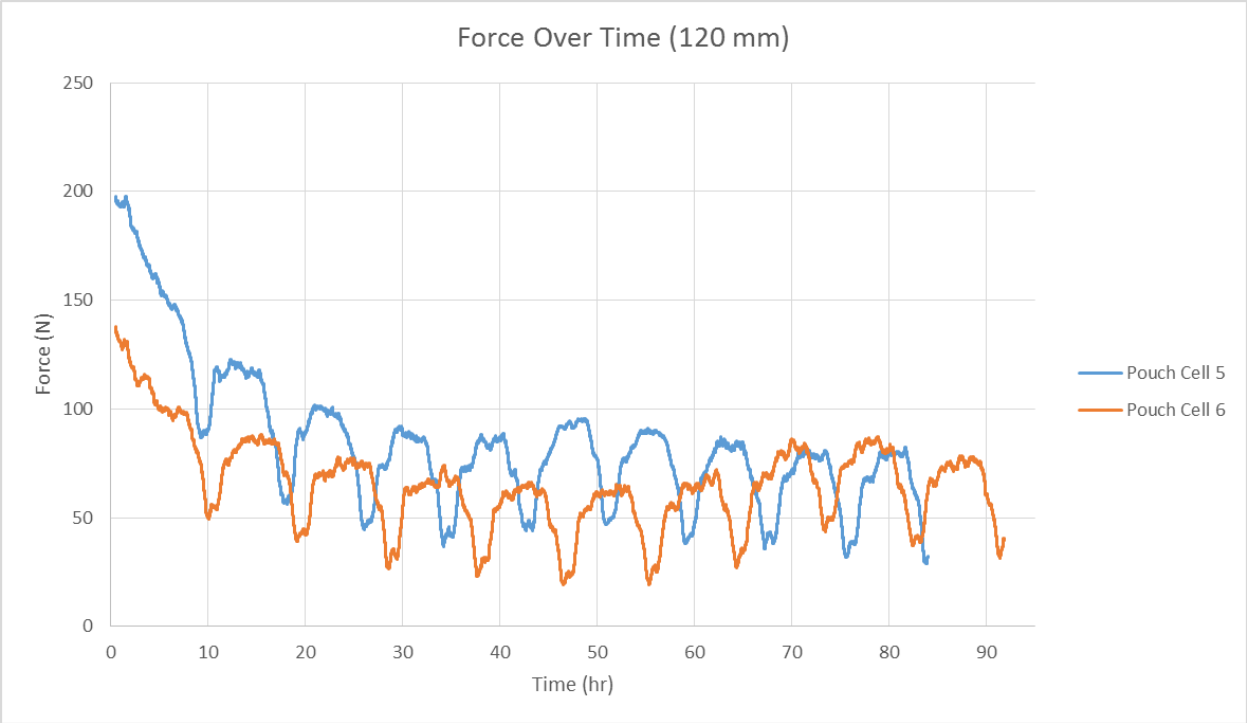

Figure 3-22: 120 mm Force over Time Curves

There was no consistently across pouch cells with regards to how the peak forces changed over time, most likely due to the age of the pouch cells. Thus, no solid conclusion regarding the relationship between force, cycling, and bending distance can be drawn.

3.3.2: Post Cycling Analysis Results & Observations

Figure 3-23 through Figure 3-25 show top and side views of Pouch Cells 2, 3, and 5 after being removed from the MTS loading frame. Prior to cutting any of the pouch cells, the local deflections were measured in order to understand some of the lasting impact of the four-point bending. While the local deflections were consistent within the pouch cell pairs, the 60 mm and 90 mm indenters produced the same level of deflection. Table 3.6 list the measured local deflections of all pouch cells post testing.

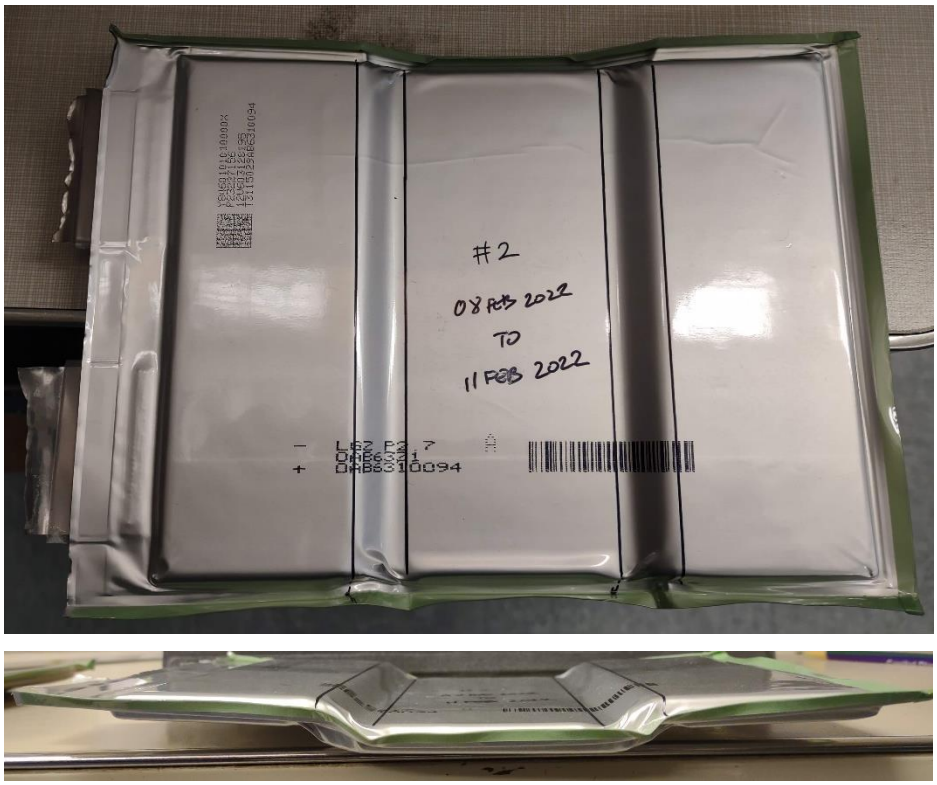

Figure 3-23: Pouch Cell #2 (60 mm)

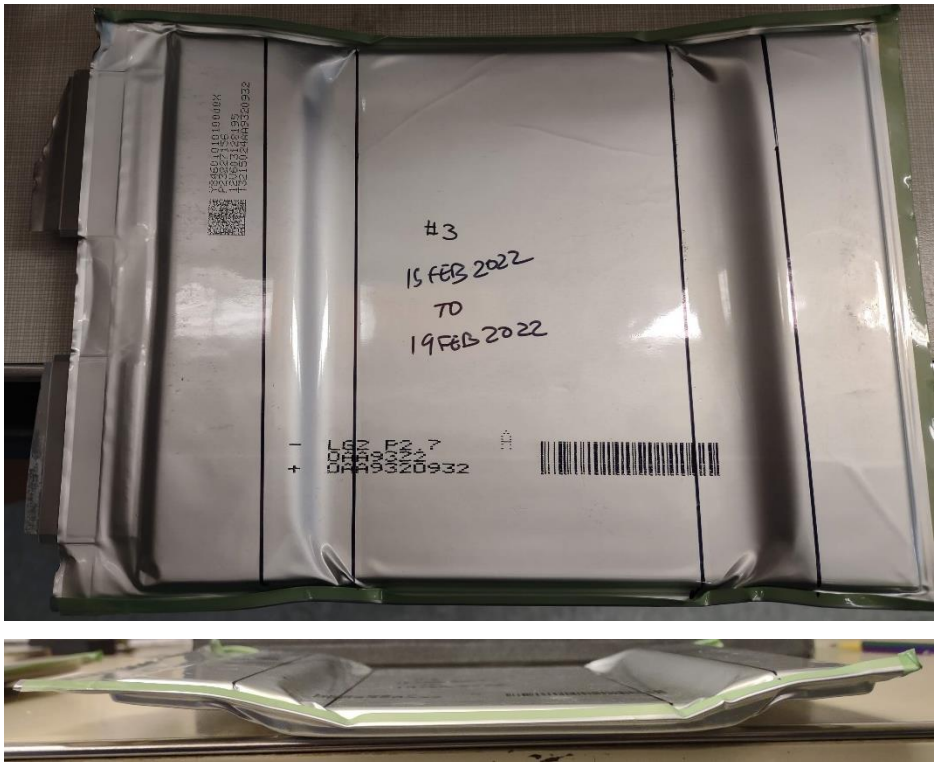

Figure 3-24: Pouch Cell #3 (90 mm)

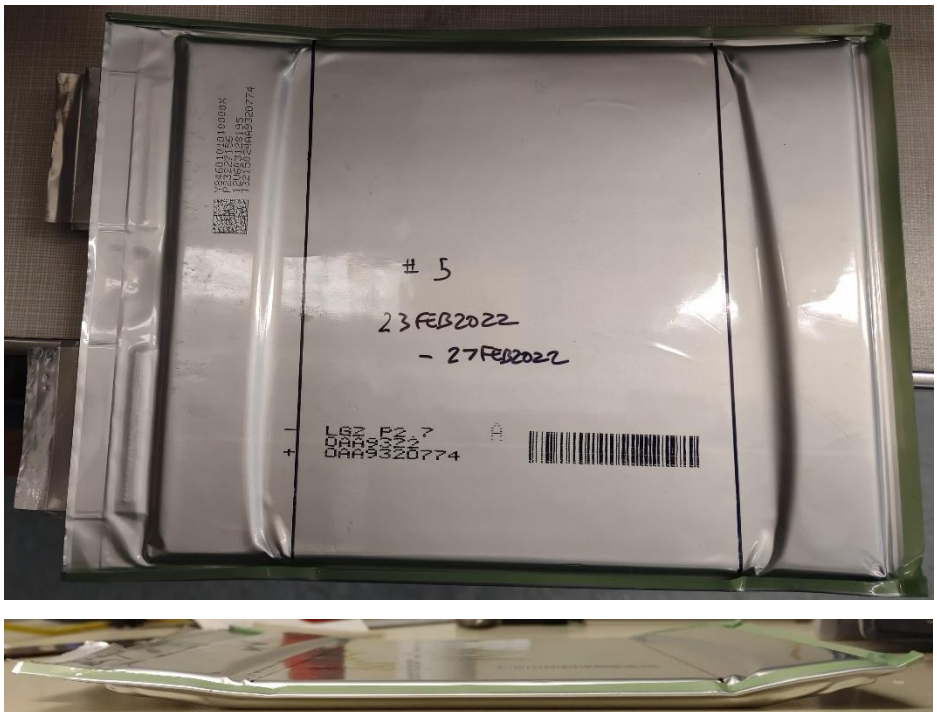

Figure 3-25: Pouch Cell #5 (120 mm)

Pouch Cell #	Post-Bending Local Deflection (mm)
1	8
2	8
3	8
4	8
5	2
6	2

Table 3.6: Post-Bending Local Deflection

Figure 3-26 and Figure 3-27 show the cross sections of pouch cells 2 and 6, respectively, after cutting them down the middle lengthwise. The original plan was to also cut pouch cell 4, however, the bent shape of pouch cells 2 and 6 were not retained during the cutting process. As pouch cell 2 was bent with the narrowest indenter, and pouch cell 6 was bent with the widest indenter, it is assumed that pouch cell 4 would also not retain its bent shape. Thus, pouch cell 4 was not cut.

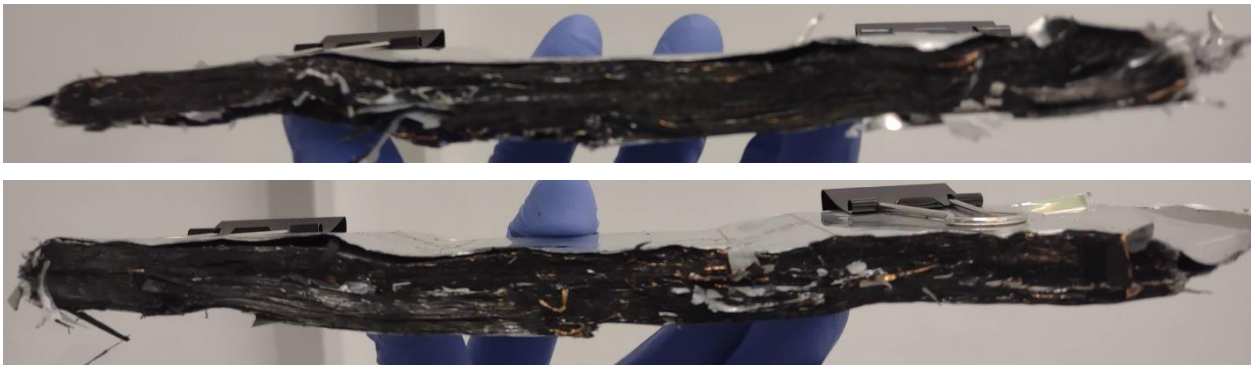

Figure 3-26: Pouch Cell #2 (60 mm) Cross Section

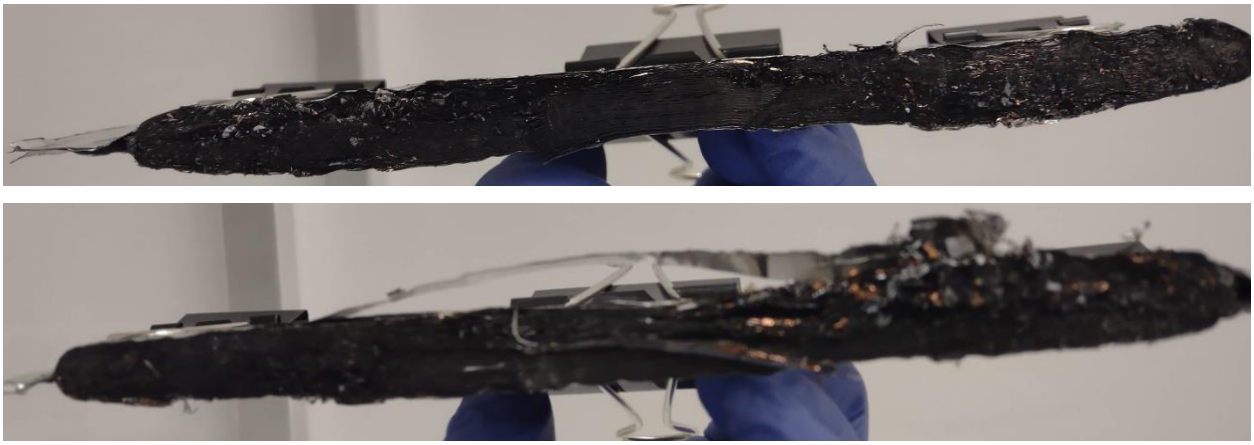

Figure 3-27: Pouch Cell #6 (120 mm) Cross Section

Chapter 4: Overall Conclusions

In addition to providing additional data to refine and validate the ICL computational model, several conclusions were derived from experimenting on the prismatic and pouch cells. First, certain types of lithium-ion cells will exert increasing pressure on their carriages as they are cycled. The prismatic cells showed a clear increase in the peak forces exerted during charging, while the pouch cells showed no consistent trend while charging under their deformed state. This has implications for the design of carriages as lithium-ion cells replace other types of batteries that may not have produced the same forces. Second, electrochemical processes over time will lead to mechanical changes within certain types of cells that may be advantageous with regard to damage resistance. The force required to break the prismatic cells increased as the number of cycles the cell was subjected to increased; however, the indentation distance was relatively constant regardless of the number of cycles. Testing lithium-ion batteries in this method can help determine if a mechanically damaged battery is dangerous to continue using by establishing a measurable limit on the damage. Finally, some electrochemical performance can be maintained despite mechanical deformation for certain types of batteries and deformations. The pouch cells, regardless of the bending indenter distances and peak bending forces experienced, maintained a constant discharge capacity over the testing period. The two implications from this conclusion are that the continued electrochemical performance of a battery may hide any mechanical deformation done to it, and that some level of mechanical deformation will not impact the electrochemical performance, again allowing the establishment of some measurable limit.

References

[1] Z. O. J. M. P. M. Yosohiaki Kato, Lithium-Ion Batteries: Overview, Simulation, and Diagnostics, Singapore: Pan Stanford Publishing Pte. Ltd., 2019.

[2] M. K. K. W. R. T. L. Celina Mikolajczak, "Lithium-Ion Hazard and Use Assessment," The Fire Protection Research Foundation, 2011.

[3] B. S. D. S. F. A. a. A. L. Jakub Zagórski, "Importance of Composite Electrolyte Processing to Improve the Kinetics and Energy Density of Li Metal Solid-State Batteries," *ACS Applied Energy Materials,* vol. 3, no. 9, 2020.

[4] US Navy, NAVSEA, 2020.

[5] "Defense Acquisitions: Success of Advanced SEAL Delivery System Hinges on Establishing a Sound Contracting Strategy and Performance Criteria," Government Accountability Office, 2007.

[6] C. P. Canvas, "Fire Deals New Setback to Navy's Heralded Mini-Sub," *The Honolulu Advisor,* 17 December 2008.

[7] M. Yeo, "Japan Commissions its First Submarine Running on Lithium-Ion Batteries," *DefenseNews,* 6 March 2020.

[8] K. Mizokami, "Japan's Jumbo New Submarine Runs on Lithium-Ion Batteries," *Popular Mechanics,* 21 October 2020.

[9] A. J. Mason, ""Material Characterization and Axial Loading Response of Pouch Lithium Ion Battery Cells for Crash Safety"," Massachusetts Institute of Technology, Cambridge, MA, 2017.

[10] N. J. Byrd, ""Combined Tensile-Compressive Biaxial Loading of Li-ion Battery Components"," Massachusetts Instittue of Technology, Cambridge, MA, 2018.

[11] MTI Corporation, *4 Channel Battery Analyzer Manual,* Richmond, CA: MTI Corporation.